the Japanese eel accumulate Zn. The ATP synthesized by the mitochondria is required for sperm flagella motility (37). Hence, Zn may have a function in mitochondrial ATP synthesis. Additionally, carbonic anhydrase (CA) is necessary for eel sperm motility, and this enzyme is expressed in the sperm membrane. CA catalyzes the reversible hydration of carbon and regulates the pH in various fluids. After spermiation, CA in the eel spermatozoa is activated after which it increases the pH and then induces sperm motility (15). CA is also known to be a Zn-binding protein, and its activity is dependent on the Zn concentration (38). Additionally, the removal of Zn from Zn-protein complexes extracted from human U87 human glioblastoma-astrocytoma cells by TPEN inhibited the function of the transcription factor, Sp1 (39). Although there is currently no information on effects of TPEN on CA activity, we speculate that TPEN may inhibit sperm motility by sequestering Zn away from this enzyme in sperm.

In conclusion, the results of our present study demonstrate that the Zn concentration in testis increases during spermatogenesis, and that Zn accumulates mainly in germ cells but not in either interstitial tissue or Sertoli cells. Our in vitro testicular organ culture experiments also demonstrated that a Zn deficiency causes the inhibition of DNA synthesis in germ cells, and induces an apoptotic response. Additionally, a Zn deficiency was found to suppress sperm motility in the Japanese eel animal model. These results suggest that Zn is an essential trace element for the maintenance and regulation of both spermatogenesis and sperm motility. However, the detailed mechanisms of Zn action during spermatogenesis remain to be clarified in further studies.

Materials and Methods

Animals. Cultivated male Japanese eels (180–200 g) were purchased from a commercial supplier and kept in a freshwater tank at 23 °C until use.

Measurement of Zn in Testis During Spermatogenesis. A previous report has indicated that hCG injection of a cultivated Japanese eel induces a complete cycle of spermatogenesis (11). Hence, these animals were injected with 1,000 IU/eel of hCG following anesthetization by ethylbenzoate. After injection, the fish were kept in a freshwater tank at 23 °C for 1, 3, 6, 9, 12, 15, and 18 days. Thereafter, hCG-injected eels (n = 5 for each day) were anesthetized and dissected, and the testes were collected and stored at −30 °C until measurement of Zn concentration. Before the experiments, testicular fragments were sampled from 5 uninjected eels as an initial control group. The testicular samples were dried for 12 h at 80 °C. For the analysis of Zn, dried testes were digested with HNO_3 in a microwave oven (ETHOS D, Milestone S.r.l.). The concentration of Zn was then measured using an inductively coupled plasma-mass spectrometer (ICP-MS; HP-4500, Hewlett-Packard).

Distribution of Zn in the Testis. We stained both the testicular fragments of the Japanese eel and the cells derived from these tissues with a Zn-specific probe. For this purpose, testis samples collected from the eels were cut into 100-μm sections in ice-cold eel Ringer's solution using a Vibratome 3000 (Vibratome). Testicular cells were also prepared according to Miura et al. (40, 13, 16) for Zn staining. Briefly, testes were harvested and testicular cells were isolated by collagenase and dispase treatments. After treatment with DNase I, testicular cells were cultured in plastic culture dishes at 20 °C overnight and both fibroblasts and interstitial cells were allowed to adhere to the bottom of the dish, thus separating these cells from germ cells and Sertoli cells. The germ cells and Sertoli cells were then collected from the culture dishes and plated in collagen-coated dishes at 20 °C overnight. After this overnight culture, only the Sertoli cells adhere to the bottom of the dish. Thereafter, germ cells were collected in a test tube, and both the germ cells and Sertoli cell preparations were used to analyze the Zn distribution. Sertoli cells and germ cells could be identified using a variety of distinguishing characteristics and specific marker expression. Sertoli cells attached and spread to the bottom of the dish, whereas germ cells did not attach and appeared spherical in shape. Furthermore, only germ cells express the progenstin receptor. We separated germ cells and Sertoli cells using this method previously (16).

Before staining of the germ cells, they were attached to a polyL-lysine coated glass slide. Testicular fragments, attached germ cells and Sertoli cells were then washed 3 times in eel Ringer's solution, and incubated with 1 μM of a permeable Zn-specific probe, Zn-AF 2DA (41) in eel Ringer's solution for 45 min at 20 °C. After this incubation, the cells were washed again in the Ringer's solution for 1 h at 20 °C and analyzed by fluorescence microscopy. The mitochondria of the spermatogonia were stained using MitoTracker Red (Invitrogen Co. Ltd.) according to the manufacturer's instructions with minor modifications before staining with Zn-AF 2DA.

In Vitro Testicular Organ Cultures. Organ cultures were prepared in accordance with the method of Miura et al. (13, 42). Male Japanese eels were dissected after anesthetization with ethylbenzoate. The testes were then collected, placed in ice-cold eel Ringer's solution and dissected into small pieces. Testicular fragments were placed on nitrocellulose membranes on top of cylindrical 1.5% agarose gels and set into a 24-well culture plate. Thereafter, 1 mL of Leibovitz' L-15 culture medium (Invitrogen Co. Ltd.) for eels (13) was added into each well with or without 0.01–1 mM $ZnCl_2$ (Zn), 0.001–0.1 mM TPEN, or 0.001–0.1 mM Ca-EDTA, which are intracellular and extracellular chelators of Zn, respectively, in combination with or without 10 ng/mL KT. The concentrations of Zn and chelators used in the in vitro experiments were based on the results obtained from the Zn measurement in the testis. Testicular fragments were incubated for 6 or 15 days and then fixed Bouin's solution for histological analysis.

Analysis of the Effects of a Mild Zn Deficiency upon Germ Cells. Testicular fragments were cultured with 0.001 mM TPEN in combination with 10 ng/mL KT, 1 ng/mL E2, and 10 ng/mL DHP for 6 or 15 days. Thereafter, testicular fragments were fixed and their histology was analyzed as described above.

Detection of Germ Cell Proliferation. The proliferation of Japanese eel germ cells was analyzed by immunohistochemical detection of 5-bromo-2-deoxyuridine (BrdU, Amersham Pharmacia Biotech) incorporation into replicating DNA. After culture for 6 or 15 days, testicular fragments were labeled with a 0.5 μl/mL BrdU solution for 18 h at 20 °C, and fixed in Bouin's solution. The fixed testicular fragments were then embedded in paraffin, cut into 4-μm sections, and subjected to immunohistochemistry with a mouse monoclonal anti-BrdU antibody.

TdT-Mediated dUTP Nick-End Labeling (TUNEL) Assay. For the detection of apoptosis, the TUNEL assay was performed. One-day cultured testicular fragments were fixed in Bouin's solution, cut into 5 μm-thick paraffin sections and then analyzed using an In Situ Cell Death Detection Kit (Roche Diagnostics, Ltd.) according to the manufacturer's instructions.

Effects of Zn on Sperm Motility. Eel sperm was collected after injection of the animals with hCG as described by Ohta et al. (43) and diluted 1:10,000 with artificial seminal plasma (149.3 mM NaCl, 15.2 mM KCl, 1.3 mM $CaCl_2$, 1.6 mM $MgCl_2$, and 10 mM $NaHCO_3$, adjusted to pH 8.2, see 43). The diluted sperm were then treated with 0.01–1 mM TPEN or 0.01–1 mM Ca-EDTA with or without 1 mM $ZnCl_2$ for 12 h at 4 °C. Thereafter, the sperm motility rate in seawater was measured as described previously (43). The duration of sperm motility was measured from 15 s after dilution in seawater until all movement had ceased completely.

Statistical Analysis. The results presented in this study are expressed as the mean ± SEM. In instances where the data did not distribute normally, these values were converted to a logarithmic scale. Differences between the means were analyzed by 1-way analysis of variance followed by a Bonferroni multicomparison test. Statistical analysis was performed using GraphPad Prism software (GraphPad Software Inc.). In all cases, significance was set at $P < 0.05$.

ACKNOWLEDGMENTS. This study was supported by Grants-in-Aid for Scientific Research and for Fellows from the Japan Society for the Promotion of Science (JSPS), and by the Global COE Program from the Ministry of Education, Culture, Sports, Science and Technology (MEXT) of the Japanese government.

1. Bedwal RS, Bahuguna A (1994) Zinc, copper, and selenium in reproduction. *Cell Mol Life Sci* 50:624–640.
2. El-Tawil AM (2003) Zinc deficiency in men with Crohn's disease may contribute to poor sperm function and male infertility. *Andrologia* 35:337–341.
3. Prasad AS (2008) Zinc deficiency. *British Med J* 326:409–410.
4. Mason KE, Burns WA, Smith JC (1982) Testicular damage associated with zinc deficiency in pre- and postpubertal rats: Response to zinc repletion. *J Nut* 112:1019–1982.

5. Merker HJ, Günther T (1997) Testis damage induced by zinc deficiency in rat. *J Trace Element* 11:19–22.
6. Boran C, Ozkan KU (2004) The effect of zinc therapy on damaged testis in prepubertal rats. *Pediatr Surg Int* 20:444–448.
7. Henkel R, et al. (2005) Molecular aspects of declining sperm motility in older man. *Fert Ster* 84:1430–1437.
8. Morisawa M, Yoshida M (2005) Activation of motility and chemotaxis in the spermatozoa: From invertebrates to humans. *Reprod Med Biol* 4:101–114.
9. Clapper DL, Davis JM, Lamothe PJ, Patton C, Epel D (1985) Involvement of zinc in the regulation of pHi, motility, and acrosome reactions in sea urchin sperm. *J Cell Biol* 100:1817–1824.
10. Stoltenberg M, et al. (1997) Autometallographic demonstration of zinc ion in rat sperm cell. *Mol Hum Reprod* 3:763–767.
11. Morisawa M, Mohri H (1972) Heavy metals and spermatozoan motility. I. distribution of iron, zinc and copper in sea urchin spermatozoa. *Exp Cell Res* 70:311–316.
12. Miura T, Yamauchi K, Nagahama Y, Takahashi H (1991) Induction of spermatogenesis in male Japanese eel, *Anguilla japonica*, by a single injection of human chorionic gonadotropin *Zool Sci* 8:63–73.
13. Miura T, Yamauchi K, Takahashi H, Nagahama Y (1991) Hormonal induction of all stages of spermatogenesis *in vitro* in the male Japanese eel (*Anguilla japonica*). *Proc Natl Acad Sci USA* 88:5774–5778.
14. Miura T, Yamauchi K, Takahashi H, Nagahama Y (1991) Human chorionic gonadotropin induced all stages of spermatogenesis *in vitro* in the male Japanese eel (*Anuilla japonica*). *Dev Biol* 146:258–262.
15. Miura T, Miura C (2001) Japanese eel: A model for analysis of spermatogenesis. *Zool Sci* 18:1055–1063.
16. Miura T, Higuchi M, Ozaki Y, Ohta T, Miura C (2006) Progestin is an essential factor for the initiation of the meiosis in spermatogenic cell of the eel. *Proc Natl Acad Sci USA* 103:7333–7338.
17. Yamaguchi S, et al. (2007) Effects of lead, molybdenum, rubidium, arsenic, and organochlorines on spermatogenesis in fish: Monitoring at Mekong Delta area and *in vitro* experiment. *Aquat Toxicol* 83:43–51.
18. Miura T, et al. (1999) Estradiol-17β stimulated the renewal of spermatogonial stem cell in males. *Biochem Biophysical Res Comm* 264:230–234.
19. Hidiroglou M, Knipfel JE (1984) Zinc in mammalian sperm: A review. *J Dairy Sci* 67:1147–1156.
20. Sørensen MB, et al. (1998) Histochemical tracing of zinc ions in the rat testis. *Mol Hum Reprod* 4:423–428.
21. Elgazar V, et al. (2005) Zinc-regulating proteins, ZnT-1, and Metallothionein I/II are present in different cell populations in the mouse testis. *J Histochem Cytochem* 53:905–912.
22. Sugihara T, Wadhwa R, Kaul SC, Mitsui YA (1999) novel testis-specific metallothionein-like protein, tesmin, is an early marker of male germ cell differentiation. *Genomics* 57:130–136.
23. Olesen C, Moller M, Byskov AG (2004) Tesmin transcription is regulated differently during male and female meiosis. *Mol Reprod Dev* 67:116–126.
24. Chi ZH, et al. (2009) ZNT7 and Zn^{2+} are present in different cell populations in the mouse testis. *Histol Histopathol* 24:25–30.
25. Guan Z, et al. (2003) Kinetic indentification of a mitochondrial zinc uptake transport process in prostate cells. *J Inorg Biochem* 97:199–206.
26. Costello LC, Guan Z, Franklin RB, Feng P (2004) Metallothionein can function as a chaperone for zinc uptake transport into prostate and liver mitochondria. *J Inorg Biochem* 98:664–666.
27. Zelewski PD, Forbes IJ, Betts WH (1993) Correlation of apoptosis with change in intracellular labile Zn(II) using Zinquin [(2-methyl-8-*p*-toluenesulphonamido-6- quinolyloxy)acetic acid], a new specific fluoprescent probe for Zn(II), *Biochem J* 296:403–408.
28. Nakatani T, Tawaramoto M, Kennedy DO, Kojima A, Matsui-Yuasa I (2000) Apoptosis induced by chelation of intracellular zinc is associated with depletion of cellular reduced glutathione levels in rat hepatocytes. *Chem-Biol Interact* 125:151–163.
29. Ho LH, et al. (2004) Labile zinc and zinc transporter ZnT4 in mast cell granules: Role in regulation of caspase activation and NF-κB translocation. *J Immunol* 172:7750–7760.
30. Jankowski-Henning MA, Clegg MS, Daston GP, Rogers JM, Keen CL (2000) Zinc-deficient rat embryos have increased caspase 3-like activity and apoptosis. *Biochem Biophysic Res Commun* 271:250–256.
31. Fukamachi Y, et al. (1998) Zinc suppresses apoptosis of U937 cells induced by hydrogen peroxide through an increase of the bcl-2/bax ratio. *Biochem Biophys Res Commun* 246:364–369.
32. Truong-Tran AQ, Carter J, Ruffin RE, Zalewski PD (2001) The role of zinc in caspase activation and apoptotic cell death. *Biometals* 14:315–330.
33. Chesters JK, Boyne R (1991) Nature of the Zn^{2+} requirement for DNA synthesis by 3T3 cells. *Experiment Cell Res* 192:631–634.
34. Freedman LP (1992) Anatomy of the steroid receptor zinc finger region. *Endocrine Rev* 13:129–145.
35. Rossi P, et al. (2004). Analysis of the gene expression profile of mouse male meiotic germ cells. *Gene Expr Patterns* 4:267–281.267–281.
36. Sørensen MB, Stoltenberg M, Danscher G, Ernst E (1999) Chelation of intracellular zinc ions affects human sperm cell motility. *Mol Human Reprod* 5:338–341.
37. Turner RM (2006) Moving to the beat: A review of mammalian sperm motility regulation. *Reprod Fert Devlop* 18:25–38.
38. Supuran CT, Scozzafava A, Casini A (2003) Carbonic anhydrase inhibitors. *Med Res Rev* 23:146–189.
39. Rana U, et al. (2008) Zinc binding ligands and cellular zinc trafficking: Apo- metallothionein, glutathione, TPEN, proteomic zinc, and Zn-sp1. *J Inorg Biochem* 102:489–499.
40. Miura T, Ando A, Miura C, Yamauchi K (2002) Comparative studies between *in vivo* and *in vitro* spermatogenesis of Japanese eel (*Anguilla japonica*). *Zool Sci* 19:321–329.
41. Hirano T, Kikuchi K, Urano Y, Nagano T (2002) Improvement and biological applications of fluorescent probes for zinc, ZnAFs. *J Am Chem Soc* 124:6555–6562.
42. Miura C, Takahashi N, Michino F, Miura T (2005) The effects of *para*-nonylphenol on Japanese eel (*Anguilla japonica*) spermatogenesis. *In Vitro Aquat Toxicol* 71:133–141.
43. Ohta H, Izawa T (1996) Diluent for cool storage of the Japanese eel (*Anguilla japonica*) spermatozoa. *Aquaculture* 142:107–118.

ORGANIC LETTERS
2009
Vol. 11, No. 13
2732–2735

Anion Sensor-Based Ratiometric Peptide Probe for Protein Kinase Activity

Kazuya Kikuchi,[†,‡,§] Shigeki Hashimoto,[†,⊥] Shin Mizukami,[‡,§] and Tetsuo Nagano*[,‡]

Graduate School of Pharmaceutical Sciences, The University of Tokyo, 7-3-1 Hongo, Bunkyo-ku, Tokyo 113-0033, Japan and PRESTO, JST Corporation, Kawaguchi, Saitama, Japan

tlong@mol.f.u-tokyo.ac.jp

Received April 7, 2009

ABSTRACT

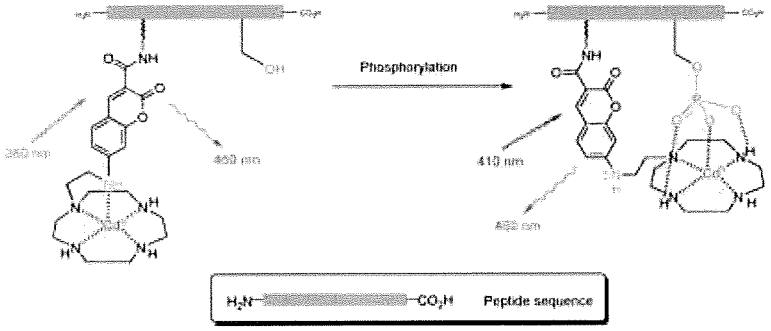

A new fluorescent sensor consisting of Cd^{II}-cylcen appended aminocoumarin and a substrate peptide for protein kinase A (PKA) has been designed. Upon phosphorylation by PKA, the metal complex moiety binds to a phosphorylated residue, which in turn displaces the coumarin fluorophore, and this event results in ratiometric change of excitation spectrum in neutral aqueous solution.

Signal transduction pathways provide mechanisms for transducing external signals to intracellular biological responses. Protein kinases modulate the activity of their target proteins by phosphorylating serine, threonine and tyrosine residues within the intact proteins in these pathways. A great number of kinases have been discovered, and the characterization of their roles in complicated signaling pathways is now a very active research area.[1] The development of an analytical tool that can enable monitoring of the temporal and spatial dynamics of cellular kinases would therefore contribute substantially to a better understanding of signal transduction mechanisms.[2]

Various approaches to monitor the activities of protein kinases have been made,[3,4] one of which is the use of fluorophore-labeled peptide substrates.[5] Traditional peptide probes contain a polarity-sensitive fluorophore near the site

[†] JST corporation.
[‡] The University of Tokyo.
[⊥] Present address: Faculty of Industrial Science and Technology, Tokyo University of Science, Oshamanbe, Hokkaido 049-3514, Japan.
[§] Present address: Graduate School of Engineering, Osaka University, 2-1 Yamada-oka, Suita City, Osaka 565-0871, Japan.

(1) *Chem. Rev.* **2001**, *101*, issue 8: Protein Phosphorylation and Signaling.
(2) (a) Eisele, F.; Owen, D. J.; Waldmann, H. *Bioorg. Med. Chem.* **1999**, *7*, 193–224. (b) Lawrence, D. S. *Acc. Chem. Res.* **2003**, *36*, 401–409.
(3) (a) Nagai, Y.; Miyazaki, M.; Aoki, R.; Zama, T.; Inouye, S.; Hirose, K.; Iino, M.; Hagiwara, M. *Nat. Biotechnol.* **2000**, *18*, 313–316. (b) Hofmann, R. M.; Cotton, G. J.; Chang, E. J.; Vidal, E.; Veach, D.; Bornmann, W.; Muir, T. W. *Bioorg. Med. Chem. Lett.* **2001**, *11*, 3091–3094. (c) Kurokawa, K.; Mochizuki, N.; Ohba, Y.; Mizuno, H.; Miyawaki, A.; Matsuda, M. *J. Biol. Chem.* **2001**, *276*, 31305–31310. (d) Ting, A. Y.; Kain, K. H.; Klemke, R. L.; Tsien, R. Y. *Proc. Natl. Acad. Sci. U.S.A.* **2001**, *98*, 15003–15008. (e) Sato, M.; Ozawa, T.; Inukai, K.; Asano, T.; Umezawa, Y. *Nat. Biotechnol.* **2002**, *20*, 287–294.
(4) (a) Ohuchi, Y.; Katayama, Y.; Maeda, M. *Analyst* **2000**, *125*, 1905–1907. (b) Ojida, A.; Inoue, M.; Mito-oka, Y.; Hamachi, I. *J. Am. Chem. Soc.* **2003**, *125*, 10184–10185. (c) Ojida, A.; Mito-oka, Y.; Sada, K.; Hamachi, I. *J. Am. Chem. Soc.* **2004**, *126*, 2454–2463.
(5) (a) McIlroy, B. K.; Walters, J. D.; Johnson, J. D. *Anal. Biochem.* **1991**, *195*, 148–152. (b) Post, P. L.; Trybus, K. M.; Taylor, D. L. *J. Biol. Chem.* **1994**, *269*, 12880–12887. (c) Higashi, H.; Sato, K.; Omori, A.; Sekiguchi, M.; Ohtake, A.; Kudo, Y. *NeuroReport* **1996**, *7*, 2695–2700. (d) Higashi, H.; Sato, K.; Ohtake, A.; Omori, A.; Yoshida, S.; Kudo, Y. *FEBS Lett.* **1997**, *414*, 55–60. (e) Yeh, R.-H.; Yan, X.; Cammer, M.; Bresnick, A. R.; Lawrence, D. S. *J. Biol. Chem.* **2002**, *277*, 11527–111532.

10.1021/ol9006508 CCC: $40.75 © 2009 American Chemical Society
Published on Web 06/04/2009

of phosphorylation, and this serves to signal the change of environment upon phosphorylation. The groups of Lawrence and Imperiali have developed chelator-appended fluorescent peptides for monitoring kinase activities.[6] Upon phosphorylation, these peptides show a significant fluorescence intensity increase owing to the formation of divalent alkaline earth metal complexes coordinated to the newly generated phosphate group and the fluorophore.

Fluorescence measurement at a single wavelength without much shift of either the excitation or emission wavelength can be influenced by artifacts associated with the microscopic imaging system. To reduce the influence of such factors, ratiometric measurement is utilized, namely, simultaneous recording of the fluorescence intensities at two wavelengths and calculation of their ratio.[7] For this approach, probes that signal phosphorylation via a shift of either excitation or emission wavelength are required.

We have designed a fluorescent anion sensor, consisting of 7-aminotrifluoromethylcoumarin as a fluorescent reporter and Cd^{II}-cyclen (1,4,7,10-tetraazacyclododecane) as an anion host.[8] This sensor molecule can detect phosphate anion species, such as pyrophosphate, with high sensitivity in aqueous neutral solution. As an extension of the anion sensor concept, we have newly designed an anion sensor-appended peptide substrate for protein kinases. Here we describe the sensing of a kinase-mediated phosphorylation event by a fluorescent peptide sensor. This novel class of peptide probe exhibited a shift of excitation spectrum upon phosphorylation, enabling ratiometric measurement of kinase activity. This technique can provide more precise data than measurement at a single wavelength, canceling out the influence of variations in instrument efficiency, content of effective dye, and so forth.

The operational concept of the peptide sensor is schematically presented in Scheme 1. This peptide sensor consists of

Scheme 1. Schematic Representation of our Peptide Sensor for Phosphorylation

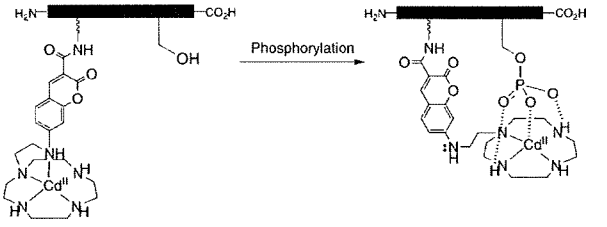

an anion sensor and a phosphorylation target peptide sequence. The sensing moiety is positioned near the target hydroxyl amino acid residue. In neutral aqueous solution, Cd^{II} of the cyclen complex is coordinated by the four nitrogen atoms of cyclen and the aromatic 7-amino group of coumarin.[9] When a negatively charged phosphate group coordinates to Cd^{II} as the fifth ligand, the aromatic 7-amino group is displaced from the metal. The anion sensor signals this replacement, because the increase of electron density of the 7-amino group induces a red shift of the excitation spectrum. We have designed peptide sensor **1** for protein kinase A (PKA) as shown in Scheme 2. The sequence of the peptide

Scheme 2. Sequence of Peptide Sensor and its Phosphorylated Standard Employed in This Study

Sensor-$(CH_2)_5$-LRRASLG-$CONH_2$ **1**

Sensor-$(CH_2)_5$-LRRApSLG-$CONH_2$ **1P**

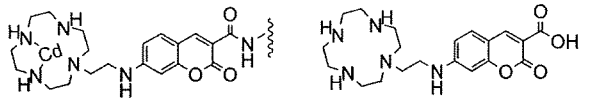

Sensor **2**

sensor is known as Kemptide and has been shown to be a good substrate for the kinase.[10] The sensing moiety is positioned at the N-terminus of the peptide through an alkyl tether, enabling recognition of a phosphorylated serine residue. We also designed a phosphorylated sensor **1P** to estimate preliminarily the extent of spectral change upon phosphorylation.

The cyclen-appended 7-aminocoumarincarboxylic acid **2** was synthesized according to the established procedure.[8] The peptide sequence was synthesized using Fmoc solid-phase chemistry on an automated peptide synthesizer and the ligand **2** was manually coupled to the amino linker. The resulting peptide conjugate was metalated with $Cd(ClO_4)_2$ to give the desired peptide sensor **1**. Phosphorylated peptide sensor **1P** was prepared by protein kinase-mediated phosphorylation of the peptide conjugate followed by metalation with Cd^{II}. The structures of **1** and **1P** were confirmed by MALDI-TOF MS (matrix assisted laser desorption/ionization-time-of-flight mass spectrometry) and quantitative amino acid analysis.

We tested the sensing ability of peptide sensor **1** by comparing the excitation spectrum with that of the phosphorylated product, **1P** (see Supporting Information). Upon phosphorylation, the excitation intensity at 360 nm decreased, whereas the intensity at 410 nm increased. The ratio of the excitation intensities (410 nm/360 nm) changed

(6) (a) Chen, C. A.; Yeh, R. H.; Lawrence, D. S. *J. Am. Chem. Soc.* **2002**, *124*, 3840–3841. (b) Shults, M. D.; Imperiali, B. *J. Am. Chem. Soc.* **2003**, *125*, 14248–14249.

(7) (a) Tsien, R. Y.; Harootunian, A. T. *Cell Calcium* **1990**, *11*, 93. (b) Kikuchi, K.; Takakusa, H.; Nagano, T. *Trends in Anal. Chem.* **2004**, *23*, 407–415.

(8) Mizukami, S.; Nagano, T.; Urano, Y.; Odani, A.; Kikuchi, K. *J. Am. Chem. Soc.* **2002**, *124*, 3920–3925.

(9) (a) Koike, T.; Watanabe, T.; Aoki, S.; Kimura, E.; Shiro, M. *J. Am. Chem. Soc.* **1996**, *118*, 12696–12703. (b) Aoki, S.; Kaido, S.; Fujioka, H.; Kimura, E. *Inorg. Chem.* **2003**, *42*, 1023–1030.

(10) (a) Kemp, B. E.; Graves, D. J.; Benjamini, E.; Krebs, E. G. *J. Biol. Chem.* **1977**, *252*, 4888–4894. (b) Kemp, B. E. *J. Biol. Chem.* **1980**, *255*, 2914–2918.

1.8-fold (from a value of 0.54 to 0.96), demonstrating that peptide phosphorylation can be detected with an anion sensor.[11]

To investigate the utility of the compound as a fluorescent probe for protein kinases, we measured the time-dependent change of the excitation spectrum of **1** treated with ATP (adenosine 5′-triphosphate) and PKA catalytic subunit (Figure 1). The phosphorylation reaction

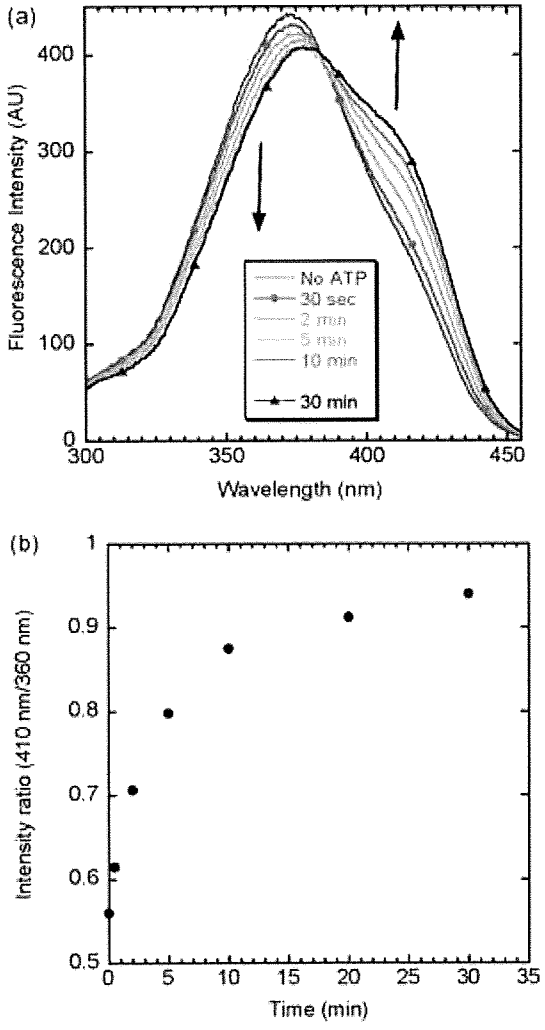

Figure 1. (a) Time course of the excitation spectra of **1** treated with PKA catalytic subunit. The peptide sensor **1** (1.3 μM) was incubated in 50 mM HEPES (pH 7.4), 5 mM $Mg(OAc)_2$ containing 4.3 nM catalytic subunit and 3.3 μM ATP at 23 ± 0.1 °C. (b) Plot of intensity ratio (410 nm/360 nm) versus reaction time.

was initiated by the addition of ATP to a mixture of **1** and the catalytic subunit. Though ATP strongly coordinates to the Cd^{II} complex of the anion sensor, addition of this organic polyanion had no significant effect on the excitation spectrum under the conditions employed.[12] As can be seen from Figure 1, the excitation spectra of **1** changed ratiometrically; the intensity at 360 nm decreased with a concomitant intensity increase at 410 nm. The ratio of excitation intensity (410 nm/360 nm) increased 1.7 fold after 30 min reaction time, and this is similar to the value obtained by comparison of the excitation spectra of authentic **1** and **1P**. The phosphorylation reaction was accelerated by increasing the quantity of kinase employed for the reaction (see Supporting Information).

We further carried out an inhibition experiment using the heat-stable inhibitor protein of PKA (PKI), which acts competitively with respect to the phosphoryl-accepting substrate (Figure 2).[13] Dose-dependent inhibition of kinase

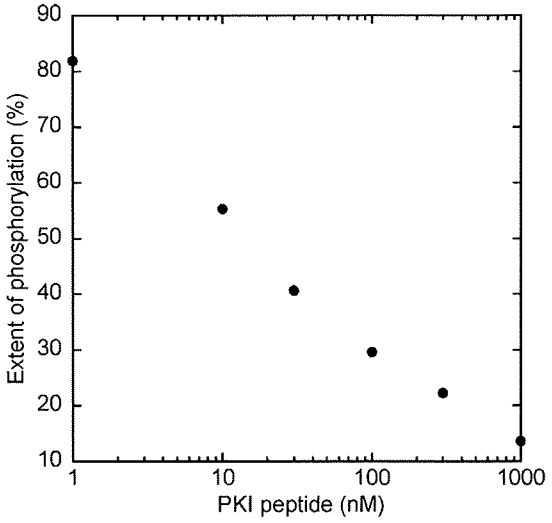

Figure 2. Titration of PKA-mediated phosphorylation of **1** with PKI peptide. The phosphorylation reaction was carried out in 50 mM HEPES (pH 7.4), 5 mM $Mg(OAc)_2$ containing 1.0 μM **1**, 4.3 nM catalytic subunit, 3.3 μM ATP and various amounts of PKI peptide at 23 ± 0.1 °C. Extent of phosphorylation (%) was determined by comparing the intensity ratio increase at the early phase of the reaction (0−5 min) with that of the control.

activity by PKI peptide was observed for phosphorylation of **1** with an IC_{50} (half maximal inhibitory concentration) of ca. 15 nM under the conditions employed. This result indicates that the ratiometric spectral change is caused by PKA-mediated phosphorylation of **1**.[14]

In conclusion, we have developed a new fluorescent probe for protein kinase based on the anion sensing principle. It has been demonstrated that this peptide probe can be used

(11) A significant shift of the absorption peak was also observed for the Cd^{II} complex of methylated compound **2** upon addition of pyrophosphate anion. Titration of the complex with pyrophosphate gave the Kd value of 53 μM.

(12) The addition of more than three equivalents of ATP to the peptide sensor **1** induced an excitation change at two wavelengtth (360 and 410 nm), which indicates the coordination of ATP to the metal complex moiety.

(13) (a) Cheng, H. C.; Kemp, B. E.; Pearson, R. B.; Smith, A. J.; Misconi, L.; Van Patten, S. M.; Walsh, D. A. *J. Biol. Chem.* **1986**, *261*, 989–992. (b) Glass, D. B.; Cheng, H. C.; Mueller, L. M.; Reed, J.; Walsh, D. A. *J. Biol. Chem.* **1989**, *264*, 8802–8810.

to continuously monitor kinase-mediated phosphorylation through intensity measurements at two wavelengths. This peptide sensor might serve as the basis for a range of anion sensor-based phosphorylation probes for many different protein kinases.

(14) Actual phosphorylation of peptide sensor **1** was confirmed by analyzing the reaction mixture, using C_{18} reverse-phase HPLC (high-performance liquid chromatography). Time-dependent production of phosphorylated product was observed when the sensor **1** was exposed to PKA catalytic subunit. The phosphorylated product co-eluted with authentic standard **1P** from the HPLC column.

Acknowledgment. We thank Prof. H. Mihara and Dr. T. Takahashi at the Tokyo Institute of Technology for technical assistance in peptide synthesis.

Supporting Information Available: Synthesis of anion sensor and peptide conjugate, fluorescence experiment, protein kinase assay. This material is available free of charge via the Internet at http://pubs.acs.org.

OL9006508

J|A|C|S COMMUNICATIONS

Published on Web 10/30/2009

Photoactive Yellow Protein-Based Protein Labeling System with Turn-On Fluorescence Intensity

Yuichiro Hori, Hideki Ueno, Shin Mizukami, and Kazuya Kikuchi*

Division of Advanced Science and Biotechnology, Graduate School of Engineering, Osaka University, 2-1 Yamadaoka, Suita, Osaka 565-0871, Japan

Received June 12, 2009; E-mail: kkikuchi@mls.eng.osaka-u.ac.jp

There has been considerable interest in bioimaging technologies for the clarification of protein functions in living systems. So far, fluorescent proteins have made a significant contribution to research on protein expression, localization, and protein−protein interaction.[1] Although various fluorescent proteins (FP) are currently known,[2] it is difficult to visualize proteins in deep tissues, because proteins emitting near-infrared fluorescence, which can pass through thick tissues, are lacking. In addition, the FP size is large (~27 kDa), and therefore, there has been a strong demand for the generation of a smaller protein tag.[3] As an alternative technology, protein labeling systems such as Halo-tag and CLIP-tag have been developed.[4] In these methods, a specific pair of a protein tag and its ligand is employed for detecting proteins of interest. The advantages of these methods are that a variety of fluorescent dyes are potentially available as labeling reagents including near-infrared probes and that the tag proteins are labeled in controlled time. However, in these systems, free probes must be removed by washing cells or purifying cell lysate to distinguish the fluorescence of bound and unbound probes. To solve this issue, our group recently reported on a fluorogenic labeling method.[5] But these tag proteins are still large.[4,5] Although there are some other techniques for protein labeling,[6] they have drawbacks in bioorthogonality or require additional enzyme for protein modification. To overcome these limitations, we utilized photoactive yellow protein (PYP) as a tag protein and developed labeling reagents for this protein, including a fluorogenic probe, which would not require any procedure for removing the free fluorescent probe.

PYP is a small, water-soluble protein found in several purple bacteria.[7] It consists of 125 amino acids (14 kDa) and binds to a natural cofactor, CoA thioester of 4-hydroxycinnamic acid, through transthioesterification with Cys69.[8] In addition to the natural cofactor, it is known that PYP binds to the thioester derivative of 7-hydroxycoumarin-3-carboxylic acid,[9] which is a fluorescent compound. Importantly, PYP and its ligands do not exist in animal cells and, thus, it is expected that PYP expressed in those cells could be bioorthogonally labeled by its exogenous ligand without any cross reaction by endogenous factors. With regard to the design of a fluorogenic labeling system, 7-hydroxycoumarin has an interesting fluorescent property as follows. Previous work shows that a coumarin derivative linked with fluorescein through a flexible linker has no or little fluorescence properties because of the intramolecular association between the dyes and their dissociation triggers the increase in fluorescence intensity.[10] Based on this principle, we designed a probe that consists of 7-hydroxycoumarin-3-carboxylic acid thioester connected to fluorescein through an ethylene glycol linker (Figure 1). It is considered that the probe in the absence of PYP is not fluorescent due to the intramolecular interaction and, once the probe binds to PYP, the coumarin is dissociated from the fluorescein because the interaction between the coumarin and PYP prevents the close contact of two fluorophores.

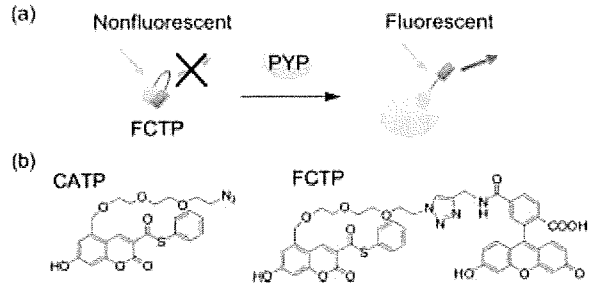

Figure 1. (a) Principle of fluorogenic labeling system based on PYP. (b) Structures of fluorescent probes, CATP and FCTP, for labeling PYP.

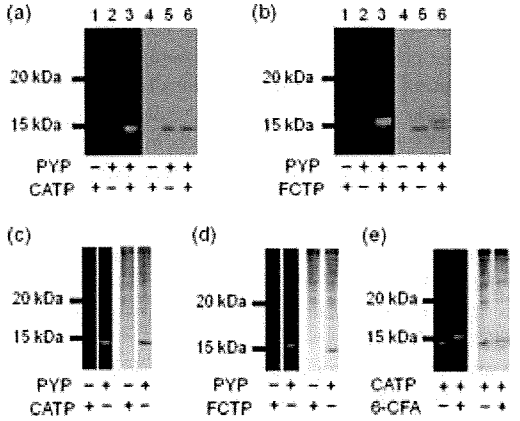

Figure 2. SDS-PAGE analyses of labeling reactions of PYP with probes, CATP and FCTP. Fluorescence and CBB-stained gel images are displayed on the left and right, respectively. PYP (10 μM) was reacted with CATP (25 μM) (a and c) or with FCTP (25 μM) (b and d). Images (c) and (d) represent the reactions in cell lysate. Image (e) represents the stepwise labeling of PYP (5 μM) with CATP (12.5 μM) and 6-CFA (200 μM) in cell lysate.

First, we synthesized CATP, which contains an azido group at the end of the linker (Figure 1b). Considering the steric hindrance, which is predicted from the structure of PYP with its natural cofactor,[11] the linker was introduced into the 5-position in the coumarin, because this position is assumed to be the 2-positon of the natural cofactor based on the structural similarity between these compounds. Then, fluorescein with an alkyne group (6-carboxy-fluorescein propalgylamide, 6-CFA) was conjugated to CATP by click chemistry to generate FCTP (Figure 1b). The probes were incubated with recombinant PYP purified from *E. coli*, and SDS-PAGE analysis was conducted to verify the binding of the probes to the protein (Figure 2a and b). In the absence of the probes, no fluorescence was detected in the gel. In the mixtures of the probes and PYP, fluorescent bands appeared, indicating that the probes bind to PYP. Interestingly, the reaction of FCTP and PYP yielded

10.1021/ja904800k CCC: $40.75 © 2009 American Chemical Society

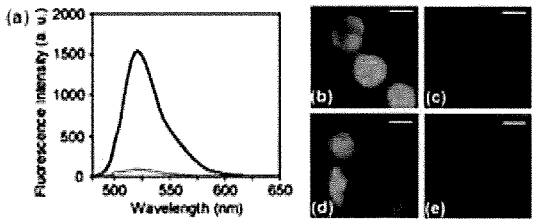

Figure 3. (a) Fluorescence spectra of FCTP (8 μM) in the absence (red dashed line) or presence (blue line) of PYP (5 μM). (b–e) Fluorescent live-cell imaging. Images (b, d) or (c, e) represent the cells that expressed or did not express PYP-PDGFRtm, respectively. The cells after incubation with CATP (5 μM; b, c) or FCTP (20 μM; d, e) are shown. Scale bars = 10 μm.

a slowly migrating band, which is regarded as FCTP-bound PYP because of its fluorescence. The binding of PYP and the probes was also confirmed by MALDI-TOF MS (Figure S1). The addition of CATP or FCTP to PYP gave the mass value of PYP bound to the individual probe, in which thiophenyl ester is replaced by thioester of Cys in the protein. The results indicate that the probes covalently bind to PYP through transthioesterification.

The binding specificity of the probes toward PYP was investigated. Labeling reactions of purified PYP were carried out in the lysate prepared from HEK293T cells. Figure 2c and d show that a single fluorescent band was detected only in the reaction mixture of PYP and each probe, confirming that PYP is specifically labeled by CATP or FCTP under this experimental condition. The influence of free thiols on the labeling reaction was also examined. The presence of a physiological concentration of glutathione (up to 10 mM) did not affect the labeling reactions (Figure S2).[13] Furthermore, the azido moiety of CATP would allow additional labeling of PYP with the second probe by click chemistry and could expand the range of the applications of this system. After the reaction of PYP and CATP in the cell lysate, 6-CFA was added to the reaction mixture in the presence of Cu^{2+} and tris(2-carboxyethyl)phosphine. Electrophoresis revealed a slowly migrating band, as is the case with the FCTP-bound PYP (Figure 2e). There were no newly appearing bands, demonstrating that the stepwise labeling reaction is quite specific.

To examine the fluorogenic properties of FCTP, the fluorescent spectra of the probes were measured (Figure 3a). In the absence of PYP, the fluorescence intensity of FCTP is very weak, suggesting that the coumarin and fluorescein dyes in the probe associate with each other. On the other hand, the binding of PYP and the probe leads to a dramatic increase in the fluorescence intensity. This increase is approximately 20-fold after 24 h of incubation. The result indicates that the coumarin dissociates from the fluorescein due to the formation of the complex between PYP and the probe. We then characterized the binding kinetics of PYP with CATP and FCTP by size exclusion chromatography and fluorescence measurement, respectively (Figures S3 and S4; see Supporting Information for the detailed procedure). The CATP reaction was almost complete within 2 h, consistent with a previous report, demonstrating the binding kinetics of a natural ligand to PYP.[12] In contrast, the binding of FCTP to PYP was slow, requiring more than 24 h to complete the reaction. One probable reason for this difference is that the intramolecular interaction in FCTP could influence its binding kinetics.

Finally, cell labeling experiments were conducted. HEK293T cells expressing PYP-PDGFRtm (the fusion protein of PYP and a transmembrane domain of platelet-derived growth factor receptor) on the cell membrane were prepared. CATP or FCTP was incubated with the cells in culture media. Fluorescence microscopy showed that fluorescent labeling by both probes occurred in the cells expressing PYP-PDGFRtm (Figures 3b and S5). No fluorescence was observed in the cells that did not express PYP-PDGFRtm, demonstrating that PYP is specifically labeled on the cell membrane by both probes. During the experiments, we noticed that CATP was cell-permeable. Therefore, intracellular imaging with CATP was also performed. After the labeling reaction of CATP and the cells expressing maltose binding protein-fused PYP (MBP-PYP) in cytosol, fluorescence was observed only in the cells expressing MBP-PYP, and not in the nonexpressing cells (Figure S5). This result clearly shows that CATP allows specific labeling of PYP inside living cells.

In conclusion, we have developed a protein labeling system, based on a small tag protein, PYP, and its fluorescent probes. The live-cell imaging and specific labeling of PYP were achieved by using CATP and FCTP. CATP has dual functions as a fluorescent probe and a chemical handle for two-step labeling. More importantly, FCTP shows fluorogenic characteristics, allowing the identification of the probe bound to its tag protein. These properties offer a more sophisticated application of this system to protein imaging studies.

Acknowledgment. This work was supported by MEXT of Japan. We thank Prof. Klaas J. Hellingwerf for providing the plasmid encoding PYP and Dr. Aya Fukuda for giving the plasmid for mammalian expression.

Supporting Information Available: Experimental procedures and supplemental results. This material is available free of charge via the Internet at http://pubs.acs.org.

References

(1) (a) Zaccolo, M. *Circ. Res.* **2004**, *94*, 866–873. (b) VanEngelenburg, S. B.; Palmer, A. E. *Curr. Opin. Chem. Biol.* **2008**, *12*, 60–65.
(2) (a) Shaner, N. C.; Steinbach, P. A.; Tsien, R. Y. *Nat. Methods* **2005**, *2*, 905–909. (b) Pakhomov, A. V.; Martynov, V. I. *Chem. Biol.* **2008**, *15*, 755–764.
(3) (a) Zhou, Z.; Koglin, A.; Wang, Y.; McMahon, A. P.; Walsh, C. T. *J. Am. Chem. Soc.* **2008**, *130*, 9925–9930. (b) Chen, I.; Ting, A. Y. *Curr. Opin. Biotechnol.* **2005**, *16*, 35–40.
(4) (a) Los, G. V.; Wood, K. *Methods Mol. Biol.* **2007**, *356*, 195–208. (b) Gautier, A.; Juillerat, A.; Heinis, C.; Corrêa, I. R., Jr.; Kindermann, M.; Beaufils, F.; Johnsson, K. *Chem. Biol.* **2008**, *15*, 128–136.
(5) Mizukami, S.; Watanabe, S.; Hori, Y.; Kikuchi, K. *J. Am. Chem. Soc.* **2009**, *131*, 5016–5017.
(6) (a) O'Hare, H. M.; Johnsson, K.; Gautier, A. *Curr. Opin. Struct. Biol.* **2007**, *17*, 488–494. (b) Wu, P.; Shui, W.; Carlson, B. L.; Hu, N.; Rabuka, D.; Lee, J.; Bertozzi, C. R. *Proc. Natl. Acad. Sci. U.S.A.* **2009**, *106*, 3000–3005. (c) Fernández-Suárez, M.; Baruah, H.; Martínez-Hernández, L.; Xie, K. T.; Baskin, J. M.; Bertozzi, C. R.; Ting, A. Y. *Nat. Biotechnol.* **2007**, *25*, 1483–1487. (d) Nonaka, H.; Tsukiji, S.; Ojida, A.; Hamachi, I. *J. Am. Chem. Soc.* **2007**, *129*, 15777–15779. (e) Adams, S. R.; Campbell, R. E.; Gross, L. A.; Martin, B. R.; Walkup, G. K.; Yao, Y.; Llopis, J.; Tsien, R. Y. *J. Am. Chem. Soc.* **2002**, *124*, 6063–6076.
(7) Kamiuchi, M.; Hara, M. T.; Stalcup, P.; Xie, A.; Hoff, W. D. *Photochem. Photobiol.* **2008**, *84*, 956–969.
(8) Kyndt, J. A.; Meyer, T. E.; Cusanovich, M. A.; Van Beeumen, J. J. *FEBS Lett.* **2002**, *512*, 240–244.
(9) van der Horst, M. A.; Arents, J. C.; Kort, R.; Hellingwerf, K. J. *Photochem. Photobiol. Sci.* **2007**, *6*, 571–579.
(10) Takakusa, H.; Kikuchi, K.; Urano, Y.; Higuchi, T.; Nagano, T. *Anal. Chem.* **2001**, *73*, 939–942.
(11) Anderson, S.; Crosson, S.; Moffat, K. *Acta Crystallogr., Sect. D* **2004**, *60*, 1008–1016.
(12) Imamoto, Y.; Ito, T.; Kataoka, M.; Tokunaga, F. *FEBS Lett.* **1995**, *374*, 157–160.
(13) Wu, G.; Fang, Y. Z.; Yang, S.; Lupton, J. R.; Turner, N. D. *J. Nutr.* **2004**, *34*, 489–492.

JA904800K

CHEMBIOCHEM

DOI: 10.1002/cbic.201000007

Noncovalent-Interaction-Promoted Ligation for Protein Labeling

Yuichiro Hori, Yuka Egashira, Ryosuke Kamiura, and Kazuya Kikuchi*[a]

Chemical labeling of proteins with fluorescent probes, isotopes, or other functional compounds provides valuable information that cannot be obtained through conventional biochemistry or molecular biology methods.[1,2] In particular, expressed protein ligation (EPL) is a powerful labeling method for analyzing protein function and structure, and has been widely applied to C-terminal labeling of proteins of interest (POI).[3] In EPL, proteins with a C-terminal thioester are linked to peptides (or proteins) with an N-terminal Cys by transthioesterification, and an amide bond is subsequently formed. The critical component of this technology is intein,[4] which is essential for generating thioester at the protein's C terminus. The major advantage of this technique is that the ligation reaction is considerably chemoselective and, thus, a desirable semisynthetic protein is reliably obtained. However, the reaction is generally inefficient and, therefore, a high concentration (mM or sub-mM) of reactants is required for efficient ligation.[2,3,5,6] Consequently, when the solubility of the reactants in water is low, a solubilization reagent, such as guanidine hydrochloride or a surfactant, is used to solubilize the reactants.[2,6] This limitation significantly hinders the application of this method to proteins that do not retain their structure and function after removal of the solubilizing reagent. In addition, barring a few exceptions,[7] this technique has not been applied to protein labeling in mammalian cell lysate or living cells because the protein expression level is not high enough for the ligation reaction. To overcome these obstacles, we developed a novel protein labeling method based on noncovalent interaction and intein-mediated ligation. This method allows efficient and specific protein labeling in cell lysate by using a low concentration range of thioester protein and synthetic peptide probe.

In order to attain efficient protein labeling, affinity tags were introduced into the reactants. This ensured that the local concentrations of the reactants would increase. As a result, it is expected that the ligation reaction would occur at low concentration. The affinity tags, Acid-a1 and Base-a1,[8] which form an antiparallel coiled coil, were chosen because these peptides are small (30 amino acids) and the interaction mechanism is well-known.[8,9] In the present research, interaction of the coiled coil was combined with the intein-mediated ligation for protein labeling (Scheme 1). Maltose binding protein (MBP) was employed as a model POI and Acid-a1 was fused to its C terminus (MBP-Acid). The intein was further connected to the C terminus of MBP-Acid to generate a fusion protein MBP-Acid-In, which could form a thioester in the C terminus of MBP-Acid. As a labeling reagent, fluorescein-conjugated Base-a1 (F-Base), which contains Cys at its N terminus, was prepared with Fmoc solid phase method. Acid-a1 with C-terminal thioester (Acid-T) was also synthesized for interaction analysis and model ligation with F-Base.

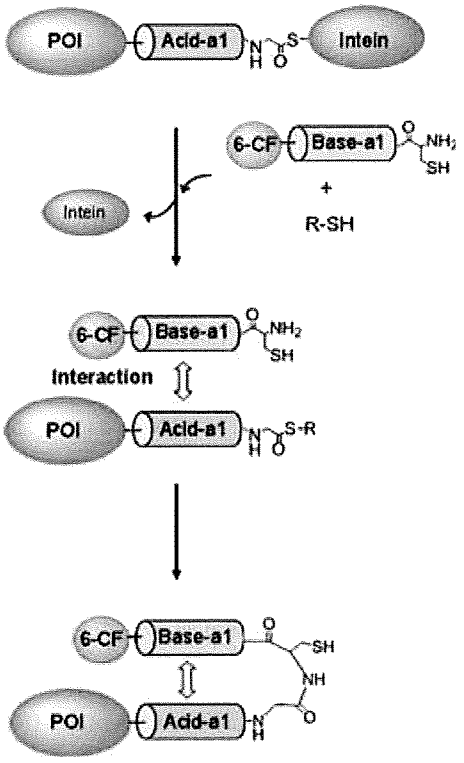

Scheme 1. Principle of protein labeling based on noncovalent coiled-coil interaction and intein-mediated ligation. Coiled coils are represented by Base-a1 and Acid-a1; POI: protein of interest; 6-CF: 6-carboxyfluorescein.

First, circular dichroism (CD) spectra were measured to determine whether coiled-coil interaction was retained despite the modification of the peptides and the fusion of Acid-a1 with protein domains. Both F-base and Acid-T showed a CD spectrum characteristic of disordered secondary structures (Figure 1 A). The addition of F-base to Acid-T resulted in a dramatic increase in negative Cotton effects at 208 and 222 nm. These results indicate that the peptides interact with each other to form α-helical structures. In contrast with the peptides, the CD spectrum of MBP-Acid-In in the absence of F-Base showed that MBP-Acid-In contains ordered secondary structures, including α-helices (Figure 1 B). This is consistent with previous reports on the crystal structures of those proteins.[10,11] The signal of MBP-Acid-In in the far-UV region intensified in the presence of F-Base; this demonstrates that the α-helix content increased. Thus, these results suggest that F-base

[a] Dr. Y. Hori, Y. Egashira, R. Kamiura, Prof. K. Kikuchi
Graduate School of Engineering, Osaka University
2-1 Yamadaoka, Suita, Osaka 565-0871 (Japan)
Fax: (+81) 6-6879-7875
E-mail: kkikuchi@mls.eng.osaka-u.ac.jp

Supporting information for this article is available on the WWW under http://dx.doi.org/10.1002/cbic.201000007.

WILEY InterScience
© 2010 Wiley-VCH Verlag GmbH & Co. KGaA, Weinheim

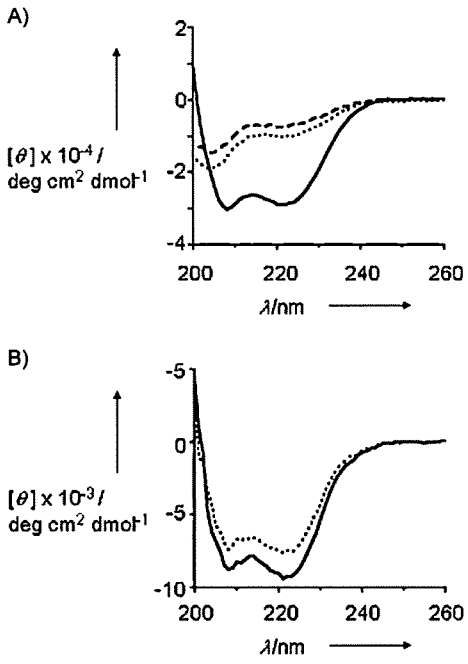

Figure 1. CD analyses of structural change in the coiled coils. A) CD spectra of F-Base (-----), Acid-T (•••••), and their complex (——). B) CD spectra of MBP-Acid-In in the absence (•••••) or presence (——) of F-Base.

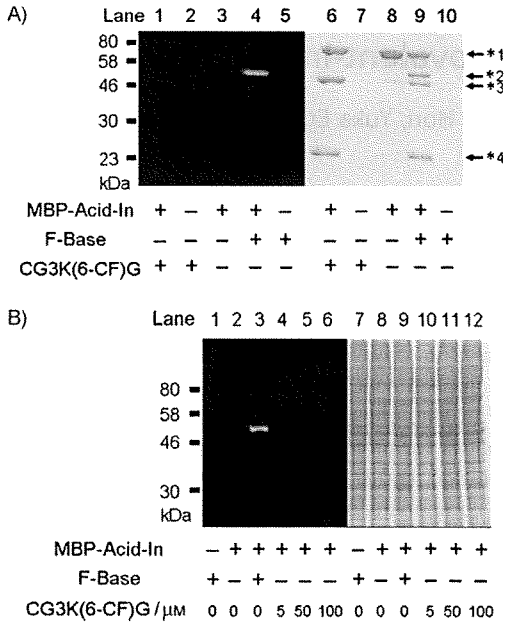

Figure 2. SDS-PAGE analyses of protein labeling experiments. Fluorescence and Coomassi Brilliant Blue-stained images are displayed on the left and right, respectively. MESNA (50 mM) was added to reaction mixtures only when they contained both MBP-Acid-In and peptide (F-Base or CG3K(6-CF)G). A) In vitro reactions of MBP-Acid-In (5 μM) with F-Base (5 μM) or CG3K(6-CF)G (5 μM) for 12 h at 25 °C. Asterisks 1–4 designate 69, 50, 46, and 23 kDa bands. B) Labeling reactions of MBP-Acid-In (5 μM) with F-Base (5 μM) or CG3K(6-CF)G (5, 50, or 100 μM) for 12 h at 25 °C in cell lysate.

binds to the segment of Acid-a1 in MBP-Acid-In and that this association induces the formation of the α-helix. Next, the model ligation reaction between F-Base and Acid-T was conducted by using low concentrations of peptides (10 μM). After a 12 h incubation period, the reaction mixture was analyzed by using HPLC (Figure S1 in the Supporting Information). Whereas the retention times of F-Base and Acid-T were 17 and 30 min, respectively, the sample after the reaction eluted at 20 min. ESI-TOF MS showed that the mass value of the eluted fraction was 8051.4, which corresponds to the theoretical mass value of the covalent ligation product (Figure S2 in the Supporting Information). This confirms that the reaction of the synthetic peptides can proceed in this concentration range.

Furthermore, the ligation reaction of F-Base and MBP-Acid-In was carried out in order to examine whether protein labeling occurs at a concentration of 5 μM. MBP-Acid-In was incubated with F-Base at 25 °C for 12 h and the labeling reaction was evaluated with SDS-PAGE. In addition to the band (69 kDa) representing MBP-Acid-In, three other bands appeared at 50, 46, and 23 kDa (Figure 2A). The band at 50 kDa corresponds to the molecular weight of F-base-conjugated MBP-Acid and was fluorescent, while the other two bands at 23 and 46 kDa can be assigned to intein and unligated MBP-Acid cleaved from MBP-Acid-In, respectively. These results indicate that MBP-Acid is labeled with F-base through a covalent bond and that the intein segment is removed as expected. This labeling reaction required MESNA (sodium 2-mercaptoethanesulfonate), which is also necessary in conventional EPL reactions.[2,3,5]

To verify the importance of the coiled-coil interaction, we carried out a labeling reaction with MBP-Acid-In and peptide CG3K(6-CF)G, which does not contain Base-a1, but has N-terminal Cys. Figure 2A shows that no fluorescent band derived from CG3K(6-CF)G was produced in lane 1 under these experimental conditions. This result clearly demonstrates that coiled-coil interaction is essential for efficient ligation. The strength of the noncovalent interaction between F-Base and MBP-Acid-In was investigated with fluorescent polarization assay in the absence of MESNA so that no ligation could occur (Figure 3). By conducting titration experiments, the dissociation constant was determined to be $(7.8 \pm 2.6) \times 10^{-8}$ M. The moderate affinity might not be sufficient for stable protein labeling with only the noncovalent interaction.[12] In contrast, in our method, the covalent ligation promoted by noncovalent interaction results in stable protein modification.

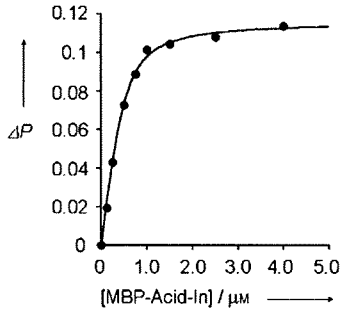

Figure 3. Determination of the dissociation constant of F-Base and MBP-Acid-In by a titration experiment. Change in fluorescence polarity (ΔP) of F-Base was plotted against the concentration of MBP-Acid-In.

 © 2010 Wiley-VCH Verlag GmbH & Co. KGaA, Weinheim

Finally, in order to clarify the specificity of the labeling, a reaction in cell lysate was performed (Figure 2B). The lysate was prepared from HEK293T cells and added to the reaction mixture. A single fluorescent band was observed in the gel only when F-base was reacted with MBP-Acid-In, demonstrating that the labeling reaction is specific. Moreover, labeling with CG3K(6-CF)G was not detected despite the incubation of the peptide with MBP-Acid-In at a higher peptide concentration (100 μM). These results indicate that the presence of the coiled-coil interaction contributes significantly to specific protein labeling as well as to the reactivity of the probe.

In conclusion, we constructed a novel system for protein labeling by utilizing a coiled-coil tag and intein. The combination of a noncovalent interaction with a covalent ligation is an effective strategy for efficient and stable modification of proteins. Importantly, the size of the coiled-coil tag is small, and specific labeling is achieved in mammalian cell lysate by using a practical concentration of peptide-based labeling reagent and target protein. These properties are highly attractive for protein detection and visualization in a complex biological environment. Hence, this technique should provide a useful approach in biochemical and biological research.

Experimental Section

See the Supporting Information for experimental details.

Acknowledgements

This work was supported by MEXT of Japan (Grants 19021028, 19036012, 20011005, 20675004 to K.K. and 20790099 to Y.H.). We thank Prof. Shigenori Kanaya and Dr. Yuichi Koga at Osaka University for the use of CD spectropolarimeter, Prof. Kazuhiko Nakatani and Dr. Chikara Dohno at Osaka University for the use of MALDI-TOF mass spectrometer, and Prof. Shiroh Futaki and Dr. Ikuhiko Nakase at Kyoto University and Dr. Tatsuto Kiwada at Kanazawa University for giving advice on peptide synthesis.

Keywords: coiled coils · fluorescence · intein-mediated ligation · protein labeling · protein modifications

[1] a) I. Chen, A. Y. Ting, *Curr. Opin. Biotechnol.* **2005**, *16*, 35–40; b) J. A. Prescher, C. R. Bertozzi, *Nat. Chem. Biol.* **2005**, *1*, 13–21; c) S. S. Gallagher, J. E. Sable, M. P. Sheetz, V. W. Cornish, *ACS Chem. Biol.* **2009**, *4*, 547–556; d) A. Gautier, A. Juillerat, C. Heinis, I. R. Corrêa, Jr., M. Kindermann, F. Beaufils, K. Johnsson, *Chem. Biol.* **2008**, *15*, 128–136; e) M. K. So, H. Yao, J. Rao, *Biochem. Biophys. Res. Commun.* **2008**, *374*, 419–423.

[2] R. R. Flavell, P. Kothari, M. Bar-Dagan, M. Synan, S. Vallabhajosula, J. M. Friedman, T. W. Muir, G. Ceccarini, *J. Am. Chem. Soc.* **2008**, *130*, 9106–9112.

[3] a) K. Alexandrov, I. Heinemann, T. Durek, V. Sidorovitch, R. S. Goody, H. Waldmann, *J. Am. Chem. Soc.* **2002**, *124*, 5648–5649; b) J. P. Pellois, M. E. Hahn, T. W. Muir, *J. Am. Chem. Soc.* **2004**, *126*, 7170–7171; c) R. R. Flavell, T. W. Muir, *Acc. Chem. Res.* **2009**, *42*, 107–116; d) D. Schwarzer, P. A. Cole, *Curr. Opin. Chem. Biol.* **2005**, *9*, 561–569.

[4] T. C. Evans, Jr., M. Q. Xu, *Biopolymers* **1999**, *51*, 333–342.

[5] a) U. Arnold, M. P. Hinderaker, B. L. Nilsson, B. R. Huck, S. H. Gellman, R. T. Raines, *J. Am. Chem. Soc.* **2002**, *124*, 8522–8523; b) P. S. Hauser, R. O. Ryan, *Protein Expression Purif.* **2007**, *54*, 227–233.

[6] D. Schwarzer, Z. Zhang, W. Zheng, P. A. Cole, *J. Am. Chem. Soc.* **2006**, *128*, 4192–4193.

[7] a) R. Y. Lue, G. Y. Chen, Y. Hu, Q. Zhu, S. Q. Yao, *J. Am. Chem. Soc.* **2004**, *126*, 1055–1062; b) L. P. Tan, R. Y. Lue, G. Y. Chen, S. Q. Yao, *Bioorg. Med. Chem. Lett.* **2004**, *14*, 6067–6070.

[8] M. G. Oakley, P. S. Kim, *Biochemistry* **1998**, *37*, 12603–12610.

[9] E. K. O'Shea, K. J. Lumb, P. S. Kim, *Curr. Biol.* **1993**, *3*, 658–667.

[10] F. A. Quiocho, J. C. Spurlino, L. E. Rodseth, *Structure* **1997**, *5*, 997–1015.

[11] T. Klabunde, S. Sharma, A. Telenti, W. R. Jacobs, Jr., J. C. Sacchettini, *Nat. Struct. Biol.* **1998**, *5*, 31–36.

[12] a) L. W. Miller, Y. Cai, M. P. Sheetz, V. W. Cornish, *Nat. Methods.* **2005**, *2*, 255–257; b) H. E. Rajapakse, D. R. Reddy, S. Mohandessi, N. G. Butlin, L. W. Miller, *Angew. Chem.* **2009**, *121*, 5090–5092; *Angew. Chem. Int. Ed.* **2009**, *48*, 4990–4992.

Received: January 5, 2010
Published online on February 19, 2010

 © 2010 Wiley-VCH Verlag GmbH & Co. KGaA, Weinheim

Cellular/Molecular

Synaptic Tagging and Capture: Differential Role of Distinct Calcium/Calmodulin Kinases in Protein Synthesis-Dependent Long-Term Potentiation

Roger L. Redondo,[1] Hiroyuki Okuno,[2] Patrick A. Spooner,[1] Bruno G. Frenguelli,[3] Haruhiko Bito,[2] and Richard G. M. Morris[1]

[1]Centre for Cognitive and Neural Systems, University of Edinburgh, EH8 9JZ, Edinburgh, United Kingdom, [2]Department of Neurochemistry, University of Tokyo Graduate School of Medicine, Bunkyo-ku, Tokyo 113-0033, Japan, and [3]Department of Biological Sciences, University of Warwick, CV4 7AL, Coventry, United Kingdom

Weakly tetanized synapses in area CA1 of the hippocampus that ordinarily display long-term potentiation lasting ~3 h (called early-LTP) will maintain a longer-lasting change in efficacy (late-LTP) if the weak tetanization occurs shortly before or after strong tetanization of an independent, but convergent, set of synapses in CA1. The synaptic tagging and capture hypothesis explains this heterosynaptic influence on persistence in terms of a distinction between local mechanisms of synaptic tagging and cell-wide mechanisms responsible for the synthesis, distribution, and capture of plasticity-related proteins (PRPs). We now present evidence that distinct CaM kinase (CaMK) pathways serve a dissociable role in these mechanisms. Using a hippocampal brain-slice preparation that permits stable long-term recordings *in vitro* for >10 h and using hippocampal cultures to validate the differential drug effects on distinct CaMK pathways, we show that tag setting is blocked by the CaMK inhibitor KN-93 (2-[*N*-(2-hydroxyethyl)]-*N*-(4-methoxybenzenesulfonyl)amino-*N*-(4-chlorocinnamyl)-*N*-methylbenzylamine) that, at low concentration, is more selective for CaMKII. In contrast, the CaMK kinase inhibitor STO-609 [7*H*-benzimidazo(2,1-a)benz(de)isoquinoline-7-one-3-carboxylic acid] specifically limits the synthesis and/or availability of PRPs. Analytically powerful three-pathway protocols using sequential strong and weak tetanization in varying orders and test stimulation over long periods of time after LTP induction enable a pharmacological dissociation of these distinct roles of the CaMK pathways in late-LTP and so provide a novel framework for the molecular mechanisms by which synaptic potentiation, and possibly memories, become stabilized.

Introduction

Activity-dependent synaptic plasticity, such as long-term potentiation (LTP) (Bliss and Lomo, 1973), is widely thought to be involved in the encoding of new information during learning. Some forms of LTP decay to baseline over a short timescale (early-LTP), whereas others, notably late-LTP, show stable synaptic potentiation for much longer (Krug et al., 1984; Frey et al., 1988). The synaptic tagging and capture (STC) hypothesis of late-LTP (Frey and Morris, 1997) asserts that LTP involves the local "tagging" of synapses at the moment of induction, that tags capture diffusely transported "plasticity-related proteins" (PRPs) synthesized in the soma or local dendritic domains, and that tag–PRP interactions are essential for stabilization of potentiation. Various lines of evidence support this framework (Frey and Morris, 1997; Martin et al., 1997; Reymann and Frey, 2007), but important open questions concern the signal-transduction pathways involved in tag setting and PRP availability.

Because relevant molecular interactions are likely to take place over several hours after LTP induction, the short time course of most LTP experiments (1–3 h) may be insufficient to monitor all the processes involved in synaptic stabilization. We therefore developed long time course *in vitro* protocols that involve (1) an interaction of strong tetanization (that sets tags and upregulates PRP synthesis) and temporally adjacent weak tetanization (which only sets tags), and (2) the rapid onset and cessation of selective kinase inhibition at appropriate times. The successful cessation of inhibition requires both rapid drug washout (i.e., the drug does not permanently bind to its target) and rapid reversibility of the action of the drug (i.e., the effect of the drug is not sustained after washout such that the normal function of the inhibited target kinase is recoverable). This double reversibility is fundamental for the dissection of heterosynaptic interactions in plasticity. These protocols also involve three independent stimulus pathways to a common pool of hippocampal neurons and exceptional control of temperature and other parameters of slice physiology to enable routine stable long-term recordings and their measurement in excess of 12 h (see Fig. 1).

The present study explores the potentially differential roles of several Ca^{2+}/calmodulin-dependent protein kinase (CaMK)

Received June 10, 2009; revised Dec. 15, 2009; accepted Jan. 6, 2010.

This work was supported by grants from the Human Frontier Science Program (R.G.M.M., H.B.), Volkswagen Stiftung (R.G.M.M.), the U.K. Medical Research Council (R.G.M.M.), the Ministry of Education, Culture, Sports, Science and Technology and Ministry of Health, Labor, and Welfare of Japan (H.B., H.O.), the Takeda Foundation (H.B.), and the Yamada Science Foundation (H.B.). We thank Tobias Bonhoeffer, Rosalina Fonseca, Mark van Rossum, and members of the Laboratory for Cognitive Neuroscience in Edinburgh for discussion and Feruza Nuritova and Colin McKenzie for earlier data.

Correspondence should be addressed to R. G. M. Morris, Centre for Cognitive and Neural Systems, University of Edinburgh, 1 George Square, EH8 9JZ, Edinburgh, UK. E-mail: r.g.m.morris@ed.ac.uk.

DOI:10.1523/JNEUROSCI.3140-09.2010

Copyright © 2010 the authors 0270-6474/10/304981-09$15.00/0

family members in the duration of LTP. Although CaMKII regulates many neuronal functions (Erondu and Kennedy, 1985; Braun and Schulman, 1995; Yamauchi, 2005), various theoretical ideas and experimental lines of evidence suggest that its activation is necessary locally for the induction and expression of LTP at synapses of the CA3 to CA1 pathway of the hippocampus (Lisman and Goldring, 1988; Malenka et al., 1989; Malinow et al., 1989). A natural question is whether CaMKII may also possess a specific role in tag setting.

In contrast, in the cell soma, calcium entry triggers activation of CaMK kinase (CaMKK) activity that stimulates CaMKIV, a nuclear kinase capable of phosphorylating Ca^{2+}/cAMP-response element binding protein (CREB) that initiates the transcription of plasticity-related genes (Bito et al., 1996; Ho et al., 2000; Kang et al., 2001). Might the pathway involving CaMKK and CaMKIV be essential for the synthesis of PRPs? To test these ideas, we examined whether reversible inhibition of different CaM kinases can specifically interfere with either the setting of tags or the synthesis of PRPs (supplemental Fig. S1, available at www.jneurosci.org as supplemental material).

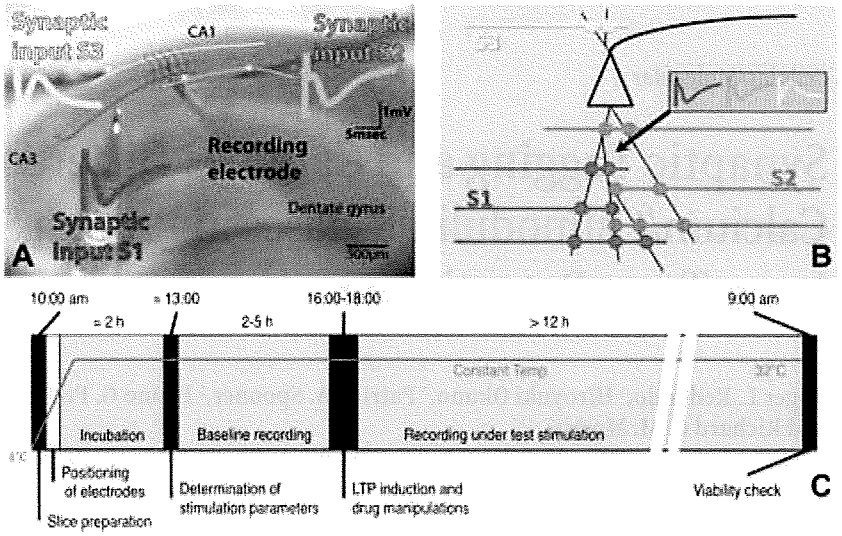

Figure 1. Experimental protocols. ***A***, The slice preparation with superimposed labels depicting the positioning of the electrodes. Color coding matches that used to identify the respective pathways throughout text. ***B***, Schematic representation depicting the independent but convergent inputs onto pyramidal cells in the CA1 used in these experiments. The recording electrode placed in the stratum radiatum of CA1 records three independent field EPSPs elicited by the activation of different populations of synapses onto the same cells. ***C***, Experimental protocol showing approximate phase lengths. Briefly, slices are cut in ice-cold aCSF and transferred to the recording chamber in which the electrodes are placed in position. Two hours of incubation allow the temperature to equalize to 32°C before input–output curves and paired-pulse stimulation tests are run to assess the optimal intensity of stimulation and confirm pathway independence, respectively. More than 2 h are still allowed to pass while baseline recordings are obtained before any drug or electrophysiological manipulations are introduced. After that, the setup returns to test-stimulation frequencies, and the experiment is allowed to develop overnight. An assessment of the viability of the slice is run the following morning (for more detailed information, see Materials and Methods).

Materials and Methods

The animals' care and maintenance and all experimental procedures were performed in accordance with United Kingdom Home Office regulations. Male Wistar rats ($n = 110$) aged 7–8 weeks were anesthetized with isoflurane and decapitated, and the brain was removed rapidly. Brain slices (400 μm) of the dorsal hippocampus were sectioned as described previously (Leutgeb et al., 2003). The hippocampal slices rested on top of eight layers of lens tissue paper (Whatman 105) placed on top of the hard surface of the slice chamber (BSC2 Scientific Systems Design; Digitimer). This ensured that the slice tissue was well soaked in the lens tissue paper while its surface remained exposed to air. All the artificial CSF (aCSF) volume held in the chamber was contained in the 2 cm wide × 2.5 cm long layers of lens tissue paper and amounted to 0.475 ml (i.e., dead volume in the chamber). All the experiments were run with the same low flow rate (0.4 ml/min) to minimize mechanical disruption of the recordings. Under these conditions, we calculate a full recycling of the aCSF every 71 s (i.e., 17 washes in 20 min). Although every drug has its own characteristics (i.e., site of action, affinity), we judged that 20 min would be enough to wash out the drugs used in these experiments. When drug washouts could be critical, alternative experiments were used to corroborate the interpretation of the result. The aCSF was prepared with the following concentrations (in mM): 124 NaCl, 3.7 KCl, 1.2 KH_2PO_4, 1.0 $MgSO_4$ (7 H_20), 2.5 $CaCl_2$, 24.6 $NaHCO_3$, and 10 D-glucose, final pH 7.4 ± 0.05. The full rig, including all the electrode holders, was heated to 32°C via the ETC system (University of Edinburgh), a procedure that prevents condensation droplets falling onto the interface chamber slices and so affecting neuronal stability.

One recording electrode, made from stainless steel rods (712700 A-M Systems), and three monopolar stainless steel electrodes (571000 A-M Systems) stimulating electrodes were positioned in CA1 (Fig. 1*A*). The slices rested for at least 2 h before preliminary recordings were taken, and no high-frequency stimulation was delivered until 5 h after dissection. The importance of this resting period for the stabilization of kinase phosphorylation levels has been emphasized previously (Ho et al., 2004; Sajikumar et al., 2005). Field EPSPs (fEPSPs) were recorded at 40–50% of the maximum amplitude obtained in an input–output curve. Test stimulation was 0.0067 Hz, 1 pulse per 150 s, resulting in one of the three channels being stimulated every 50 s (0.02 Hz). This low rate was chosen to allow the activity rates of kinases and other molecules to drop to a resting state between stimulation (Sajikumar et al., 2005). At this low rate of stimulation, hippocampal slices react more slowly to drugs such as anisomycin than at faster rates (Fonseca et al., 2006; Sajikumar et al., 2008). Also importantly, test stimulation activates NMDA receptors and the molecular cascades linked to it (Navakkode et al., 2007). Minimizing the impact of test stimulation is in the interest of recording stability (Schurr et al., 1986) as well as reproducibility of the data from experiment to experiment.

Data (fEPSP slope) was normalized to a baseline calculated over 60 min before the first tetanization. The "strong" tetanization protocol consisted of three trains of 100 pulses at 100 Hz delivered at 10 min intervals (300 pulses in total). The "weak" tetanization protocol was a theta burst consisting of four trains, at a 200 ms interval, consisting of five pulses at 100 Hz (20 pulses in total). Pathway independence was tested by using standard pair-pulse stimulation protocols that alternated between the two stimulating pathways placed in the stratum radiatum of CA1 (50 ms interpulse interval). The experiment proceeded provided this procedure failed to show paired-pulse facilitation (PPF). Normal PPF was detected when PPS was delivered to either of the two pathways as would be expected when the same presynaptic fibers are recruited by both pulses (data not shown). In addition to this control for pathway independence, the induction of LTP in one pathway fail to induce any LTP on the other two pathways in all our experiments. Pathway convergence is assumed from the limited area of sensitivity of the extracellular recording electrode, from the layered anatomy of the hippocampus, and from the observation of heterosynaptic plasticity dependent on intracellular processes (Schwartzkroin and Wester, 1975; Andersen et al., 1977; Frey and Morris, 1997).

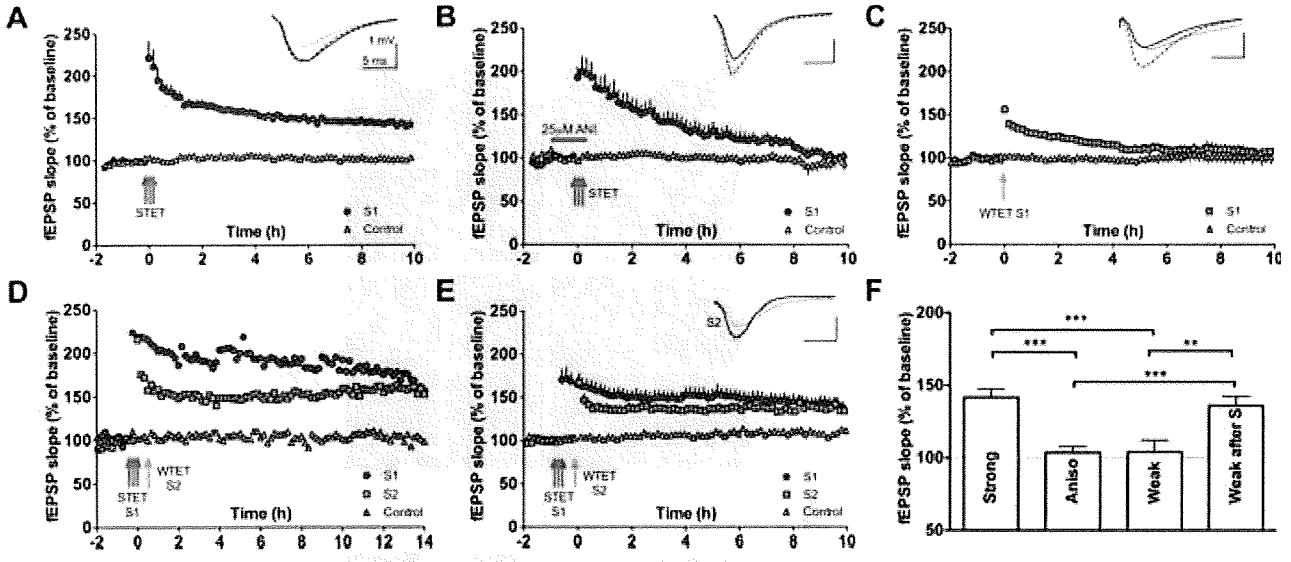

Figure 2. Synaptic tagging and capture in the stratum radiatum of CA1 pyramidal cells. ***A***, Strong tetanization (STET) (3 trains of 100 pulses at 100 Hz given 10 min apart) produces an increase in the synaptic response that lasts 10 h (late-LTP) relative to both the pretetanization baseline ($t = 8.0, p < 0.01$; red symbols) and a nontetanized control pathway ($t = 4.9, p < 0.01$; yellow symbols). This strongly induced LTP was stable over time (comparison of 2 and 10 h time points; $t = 2.0, p \geq 0.05$). The insets in each graph represent typical EPSP traces per stimulated input 30 min before (dotted line), 30 min after (broken line), and 10 h after (full line). Calibration: 1 mV, 5 ms ($n = 7$). ***B***, Late-LTP is not maintained when a strong tetanus is given in the presence of the protein synthesis blocker anisomycin. The potentiation declined to baseline after 10 h (S1 vs baseline; $t = 0.15, p \geq 0.05; n = 9$). ***C***, A weak tetanus (WTET) (4 trains of 5 pulses at 100 Hz given 200 ms apart) elicits LTP present at 2 h (S1 vs control pathway; $t = 4.3, p < 0.01$) that returns to baseline strength after 3 h (S1 vs control pathway; $t = 1, p \geq 0.05; n = 6$). ***D***, ***E***, Early-LTP (orange symbols) is rescued into late-LTP (S2 vs control pathway at 10 h; $t = 3.4, p \leq 0.01$) when one set of synapses receives the weak tetanus 20 min after another set of synapses onto the same population of pyramidal cells has received a strong tetanus (***D***, single experiment; ***E***, pooled data; $n = 8$). ***F***, Bar graph showing differences in the level of potentiation 10 h after stimulation between the four different conditions presented in ***A–E*** (one-way ANOVA, $F = 15.13, p < 0.001$). The change in synaptic efficacy remaining 10 h after the strong tetanization of a set of synapses is significantly higher than when the tetanization takes place under the presence of 25 μM anisomycin ($t = 5.45, p < 0.001$) and higher than the potentiation remaining after weak tetanization ($t = 4.53, p < 0.001$). In a similar way, the potentiation left after 10 h in a pathway weakly stimulated before strong tetanization was given to an independent but convergent set of synapses is greater than if the weak tetanization is given alone ($t = 3.92, p < 0.01$) or if a strong tetanus is given together with anisomycin ($t = 4.81, p < 0.001$). Error bars indicate SEM. $^{**}p < 0.01$; $^{***}p < 0.001$. Multiple *t* tests were comparisons done with Bonferroni's correction.

KN-93 (2-[*N*-(2-hydroxyethyl)]-*N*-(4-methoxybenzenesulfonyl)amino-*N*-(4-chlorocinnamyl)-*N*-methylbenzylamine), Myr-AIP (*N*-Myr-Lys-Lys-Ala-Leu-Arg-Arg-Gln-Glu-Ala-Val-Asp-Ala-Leu-OH), and KN-92 (2-[*N*-(4′-methoxybenzenesulfonyl)]amino-*N*-(4′-chlorophenyl)-2-propenyl-*N*-methylbenzylamine phosphate) were obtained from Calbiochem, anisomycin and D-AP-5 were from Sigma, and STO-609 [7*H*-benzimidazo(2,1-a)benz(de)isoquinoline-7-one-3-carboxylic acid] was from Tocris Bioscience.

The average values of the slope function of the fEPSP (millivolts per milliseconds) for each time point were analyzed using paired (within-group) and unpaired (between-group) *t* tests; $p < 0.05$ was considered as statistically significant, but we show more exacting levels of significance in many cases. Parametric tests were used because the data conformed to a Gaussian distribution, but analysis using nonparametric tests (Mann–Whitney and Wilcoxon's tests) supported the same conclusions. To measure the stability of late-LTP, we compared the absolute level of potentiation relative to the baseline 2 h after its induction with the level remaining after 10 h. This measure distinguishes stability and amplitude in a manner that is not usually considered. Specifically, it distinguishes between "stable late-LTP" and "decaying LTP that still shows potentiation at the end of the experiment" because the latter may arise if there is strong initial expression of LTP. We hope that this measure clarifies the difference between strength and persistence of LTP.

Hippocampal dissociated cultures were prepared from neonatal Wistar rats and cultured on coverslips as described previously (Bito et al., 1996; Kawashima et al., 2009). At 20–21 d *in vitro*, at which synaptic network in the culture was well developed, neurons were silenced with 2 μM TTX for 2 h and treated with various concentrations of kinase inhibitors (KN-93 or STO-609 in 0.1% DMSO) for 30 min in Tyrode's solution (in mM: 124 NaCl, 2.5 KCl, 1.0 NaH_2PO_4, 2.0 $CaCl_2$, 2.0 $MgCl_2$, 24.6 $NaHCO_3$, 30 D-glucose, and 20 HEPES, pH 7.4). The cultures were then stimulated with 10 μM glutamate/100 μM glycine/1 μM TTX in 0 Mg^{2+} Tyrode's solution for 3 min in the presence of the inhibitors. After stimulation, neurons were immediately fixed in chilled methanol for 5 min, followed by ice-cold 4% paraformaldehyde/4% sucrose/PBS for 5 min.

Immunocytochemistry was performed essentially as described previously (Kawashima et al., 2009). Briefly, the fixed cells were washed, permeabilized, and incubated in a blocking solution (3% BSA/0.3% Triton X-100/PBS) with a phosphatase inhibitor cocktail (PhosSTOP; Roche). The cells were then reacted with primary antibodies in the blocking solution. The primary antibodies used were anti-phosphorylated-CREB (pCREB) [rabbit monoclonal antibody (mAb); Epitomics] and anti-MAP2 (mouse mAb; Sigma) or anti-pCaMKII (rabbit polyclonal antibody; Promega) and anti-CaMKIIα (mouse mAb; Invitrogen). After the wash, the primary antibodies were labeled with anti-mouse AlexaFluor488-conjugated and anti-rabbit AlexaFluor594-conjugated secondary antibodies. The cells were then washed, stained with 4′,6′-diamidino-2-phenylindole (DAPI), and mounted on slides.

Fluorescence images were acquired using a confocal laser scanning microscopy or an EM-CCD camera mounted on an inverted microscope. To obtain two-dimensional images, a *z*-stack of multiple confocal section images were acquired using an LSM510 META confocal laser microscope (Carl Zeiss), and then the stack data were projected into single planes by a summation algorithm. The projected images were color coded and shown. To quantify fluorescent pixel intensities, single-plane images were directly acquired using an EM-CCD camera (Andor) mounted on an inverted microscope (IX81; Olympus), to take advantage of the higher sensitivity and dynamic range of the camera. For quantification, regions of interest (ROIs) were set on neuronal nuclei, which were defined by DAPI and MAP2 staining, for pCREB immunoreactivity (n = 89–154 neurons per condition), and on dendritic spines defined based on total CaMKIIα immunoreactivity for pCaMKII (n = 127–203 spines from 9–12 neurons). Average intensity in each ROI was calculated using the

MetaMorph software (Universal Imaging Corporation), and dose-dependent curves were drawn using the Prism software (GraphPad Software). The values under TTX condition and stimulation without drugs (DMSO only) were defined as basal (0%) and maximum (100%) activities, respectively. The image analyses were done in a blind manner.

Results

Synaptic tagging and capture

Conventional experiments examining late-LTP relative to a nontetanized baseline cannot, alone, isolate the putatively distinct roles played by different signal-transduction pathways in synaptic tagging, the availability of PRPs, or the putative capture process. Two-pathway experiments deploying what we shall call "weak-before-strong" and "strong-before-weak" protocols, in which weak and strong tetanization are given sequentially to two independent pathways, are essential to examine the dissociations that are central to this study. Ideally, to perform long experiments in which two independent pathways are tetanized at some point, it is desirable to have a three-pathway configuration with a third nontetanized pathway to monitor the overall stability of the slice preparation (Fig. 1). We incorporated this to enable potentiated pathways to be compared with the control pathway at various time points rather than only make comparisons to pretetanus baselines. We began by establishing that our tetanization protocols are successful in producing late-LTP that is exceptionally stable over time.

LTP lasting >10 h with an absolute level of ~142% (at 10 h) relative to both the pretetanization baseline ($p < 0.01$) and higher than a nontetanized control pathway ($p < 0.01$) was routinely obtained after strong tetanization (Fig. 2*A*). This persistent late-LTP was sensitive to the presence of the protein synthesis blocker anisomycin at induction; in addition to displaying fEPSP decay over time with anisomycin, there was no difference between fEPSP slope at 10 h after tetanus (S1) and the pretetanus baseline ($p > 0.05$) nor between S1 and the control pathway at 10 h after tetanus ($p \geq 0.05$). Using our novel "stability" measure (described in Materials and Methods), the within-pathway decline in the level of potentiation in S1 from 2 to 10 h was significant ($p < 0.01$) (Fig. 2*B*). The NMDA receptor antagonist D-AP-5 (25 μM) blocked LTP induction (S1 relative to control; $p > 0.05$). After washout and 1 h after the previous tetanus, a second strong tetanization was delivered to confirm the reversibility of the NMDA receptor block, and, under these conditions, late-LTP could be induced ($p < 0.05$) (supplemental Fig. S2, available at www.jneurosci.org as supplemental material).

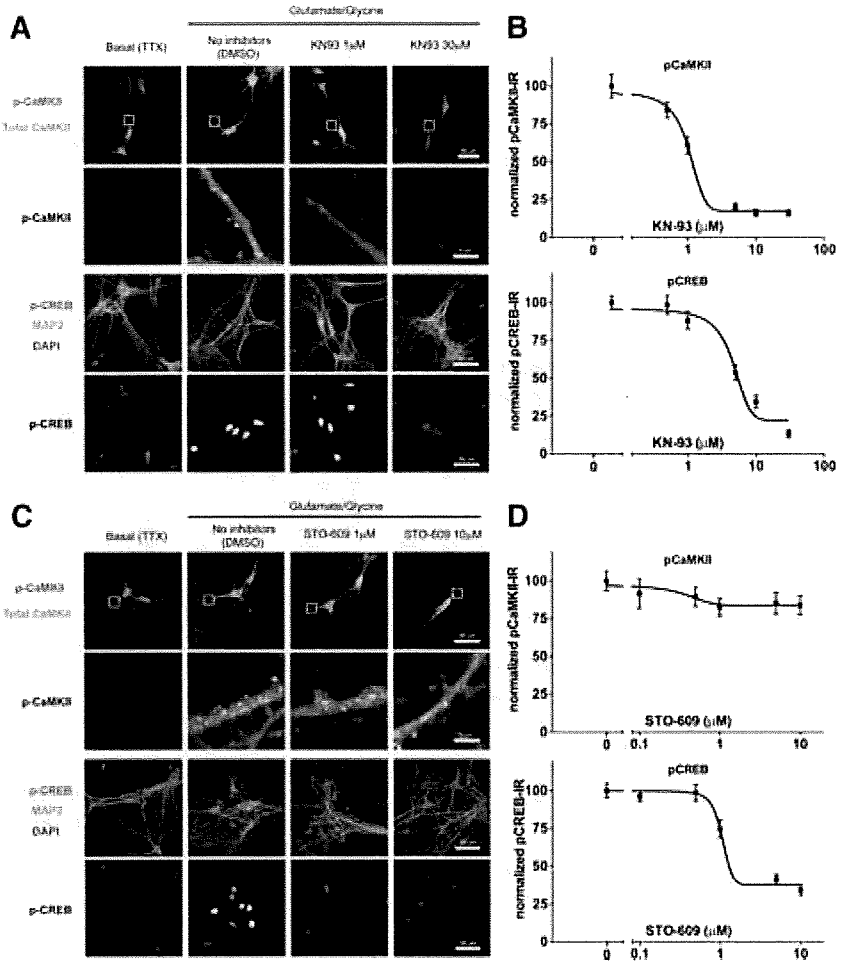

Figure 3. Dose-related effects of KN-93 and STO-609 on phosphorylation of CaMKII and CREB. ***A***, Top, Effects of kinase inhibitors on pCaMKII (top rows) and on pCREB (bottom rows) in dissociated hippocampal culture. Neurons were stimulated with bath application of glutamate/glycine in the presence of KN-93. pCaMKII immunoreactivity in dendritic spines was measured for quantification. Framed areas in the top row were expanded and pCaMKII channel was shown at the bottom in a pseudocolor scale. pCREB immunoreactivity was quantified in neuronal nuclei that were identified with MAP2 and DAPI staining. The pCREB channel was separately shown in a pseudocolor scale below. ***B***, Differential dose responses of KN-93 on distinct CaMK pathways in culture neurons. Top, Effects of KN-93 on CaMKII autophosphorylation at Thr-286. Immunoreactivity (IR) for pCaMKII was quantified in dendritic spines and displayed as a function of KN-93 concentration. The ordinate represents basal (no stimulation, 0%) to maximum (stimulated without inhibitors, 100%) activities. Bottom, Effects of KN-93 on CREB phosphorylation at Ser-133. Suppression of pCREB immunoreactivity in the neuronal nuclei was displayed. Note greater sensitivity of KN-93 for CaMKII. ***C***, Effects of STO-609 on pCaMKII and on pCREB in dissociated hippocampal culture. Neurons were stimulated with bath application of glutamate/glycine in the presence of STO-609. pCaMKII immunoreactivity in dendritic spines was measured for quantification. Framed areas in the top row were expanded and pCaMKII channel was shown at the bottom in a pseudocolor scale. pCREB immunoreactivity was quantified in neuronal nuclei that were identified with MAP2 and DAPI staining. The pCREB channel was separately shown in a pseudocolor scale below. ***D***, Differential dose responses of STO-609 on distinct CaMK pathways in culture neurons. Top, Effects of STO-609 on CaMKII autophosphorylation at Thr-286. Bottom, Effects of STO-609 on CREB phosphorylation at Ser-133. Error bars indicate SEM.

Thus, strong tetanization induced an NMDA receptor-dependent, anisomycin-sensitive late-LTP. Conversely, potentiation induced by weak tetanization was clearly present at 2 h (25% above baseline; $p < 0.01$), but this early-LTP declined within 6 h and was absent after 10 h ($p > 0.05$, relative to control) (Fig. 2*C*). Using our measure of LTP stability over time, comparison of the 2 and 10 h time points showed a significant decline in the weakly tetanized synapses ($p < 0.05$).

To demonstrate STC, the strong tetanus protocol was then given to pathway S1, and, 20 min after the last 100 Hz train, a weak tetanus was applied to a second independent but conver-

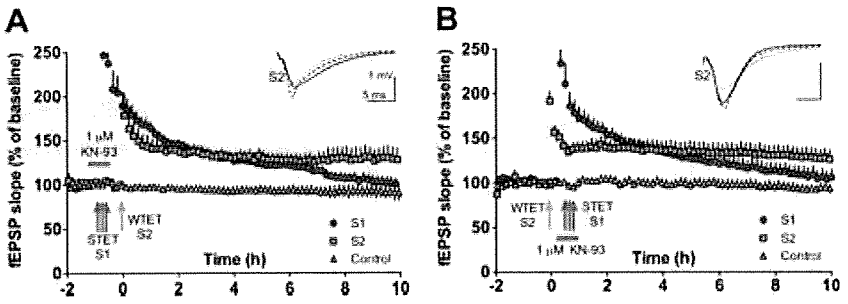

Figure 4. KN-93 dissects a role for CaMKII in a synapse-specific process necessary for late-LTP. *A*, Strong tetanization (STET) in the presence of 1 μM KN-93 (pathway S1) induces LTP that decays to baseline over 10 h (S1 vs control pathway, $t = 1.7, p \geq 0.05$; red symbols), whereas an independent set of weakly tetanized (WTET) synapses (S2; orange symbols) successfully shows stable potentiation for 10 h after tetanus (S2 relative to baseline at 10 h after tetanus, $t = 3, p \leq 0.05$; S2 at 2 vs 10 h, $t = 1.2, p \geq 0.05$; $n = 8$). *B*, In a weak-before-strong protocol, early-LTP is still rescued to late-LTP (S2 vs control pathway, $t = 3.2, p \leq 0.05$), although late-LTP fails to be maintained in those synapses tetanized in the presence of 1 μM KN-93 (S1 vs control pathway, $t = 1.4$, $p \geq 0.05$; S1 at 2 vs 10 h, $t = 4.7, p \leq 0.01; n = 7$). Error bars indicate SEM. Symbols as in Figure 2.

gent pathway S2 (strong-before-weak protocol). In a single representative experiment, late-LTP was observed on both pathways lasting >14 h (Fig. 2*D*). The group data of a series of experiments ($n = 8$) revealed that pathway S2 maintained its potentiated state for at least 10 h. This was shown by comparing S2 with the third, control pathway ($p \leq 0.01$) and by establishing stability over the 2–10 h posttetanization time period (S2 at 2 vs 10 h, $p \geq 0.05$) (Fig. 2*E*). This stable late-LTP on S2 also differed from that seen on weakly tetanized pathways in slices that did not receive heterosynaptic strong stimulation (compare S2 in Fig. 2*E* with *C* at 10 h: $t = 3.4$, $p < 0.05$).

These results confirm previous findings (Frey and Morris, 1997, 1998a) and extend them through our use of three pathways and a monitoring time after LTP of >8 h, additional features essential for the later phases of experimentation.

Differential sensitivity of phosphorylated CaMKII and CREB to varying concentrations of KN-93 and STO-609

The CaMK inhibitor KN-93 has a broad spectrum of specificity for inhibiting CaM kinases, but the dose–response profile differs between CaMK subtypes. To verify the sensitivity of both CaMKII-mediated and CaMKK/CaMKIV-mediated phosphorylation processes to KN-93, cultured hippocampal neurons were exposed to robust glutamate-induced stimulation of phosphorylation, and we measured immunoreactivities for both pCaMKII (as a readout of CaMKII activity) and pCREB (as a functional readout of CaMKIV activation), in the presence of graded concentrations of KN-93 (Fig. 3*A*). Both pCaMKII and pCREB were blocked at a high concentration (e.g., 30 μM). The dose–response relation for inhibition of pCREB was rightward shifted relative to pCaMKII inhibition (Fig. 3*B*), consistent with the ideas that (1) CaMKII phosphorylation is more sensitive to KN-93, and (2) a higher concentration of KN-93 should be necessary to fully block PRP synthesis and availability. It is important to note that a low (1 μM) concentration of KN-93 has been shown previously to be sufficient to impair synaptic plasticity in brain slices (Hansel et al., 2006). CaMKII, with a K_i of 370 nM (Sumi et al., 1991), should be effectively blocked at this concentration, whereas the activity of other CaM kinases, such as CaMKIV, would be far less potently inhibited (Ishida et al., 1995).

In contrast, immunocytochemical assays using cultured neurons revealed that high concentrations of STO-609 (>1 μM) are capable of blocking phosphorylation of CREB, because CaMKK lies upstream of the CREB kinase CaMKIV but does not interfering with CaMKII phosphorylation (Fig. 3*C*,*D*).

KN-93 at 1 μM blocks late-LTP but allows a separate and weakly tetanized pathway to display late-LTP

Using the critical strong-before-weak protocol, KN-93 (1 μM) was applied during the strong tetanization of one pathway (S1, to block late-LTP) and washed out, and, 20 min later, weak tetanization was delivered to pathway S2. KN-93 completely blocked late-LTP on pathway S1 (compare pretetanus baseline at 10 h and control pathway in Fig. 4*A*, $p > 0.05$). In contrast, pathway S2 weakly stimulated 20 min after KN-93 washout maintained late-LTP for at least 10 h (Fig. 4*A*, $p < 0.05$) and was stable from 2 to 10 h ($p > 0.05$). The level of potentiation in the two pathways "crossed over." This is a critical observation, because it implies that PRPs must have been made available to synapses of the S2 pathway. Because S2 was weakly tetanized, the PRPs were likely upregulated by the strong tetanization of pathway S1. Given that pathway S1 decayed to baseline, it follows that 1 μM KN-93 must have selectively blocked a process critical for late-LTP but distinct from PRP availability, namely tag setting.

We confirmed these findings using the alternative weak-before-strong protocol. The weakly tetanized pathway (S2) showed sustained late-LTP over 10 h ($p < 0.05$), despite the decay to baseline (and crossover) of the potentiation induced by the later strong tetanization in the presence of KN-93 of the S1 pathway (compare baseline and control pathway in Fig. 4*B*, $p > 0.05$). Together, these experiments suggest that CaMKII, being sensitive to lower concentrations of KN-93, might play a major role in tag setting, whereas its role in the regulation of PRP availability might be more limited.

This suggestion relies on the actions of a general CaMK inhibitor that was used at a low dose at which it preferentially inhibits CaMKII. To strengthen the view of a specific role for CaMKII in tag setting, we also tested the effect of a myristoylated, cell-permeant, form of a CaMKII-selective inhibitory peptide, AIP (Ishida et al., 1995). We first confirmed that Myr-AIP can strongly inhibit pCaMKII formation in cultured neurons in the absence of any effect on pCREB (supplemental Fig. S3*A*,*B*, available at www.jneurosci.org as supplemental material). Next, using a standard strong-before-weak STC protocol, we tested whether the rescue of early-LTP into late-LTP (supplemental Fig. S3*C*, available at www.jneurosci.org as supplemental material) would be compromised by the presence of 5 μM Myr-AIP during early-LTP induction. Myr-AIP was bath applied during the weak tetanization of S2. In keeping with our previous results with a low concentration of KN-93, pathway S2 failed to show late-LTP [compare with baseline in supplemental Fig. S3*D* (available at www.jneurosci.org as supplemental material), $p > 0.05$]. We also note that early-LTP is diminished in the presence of Myr-AIP, consistent with previous results (Sanhueza et al., 2007). This indicates that Myr-AIP blocked the ability of PRPs generated in pathway S1 to convert a subsequent early-LTP in S2 into late-LTP, i.e., it compromised tag setting. Together, these data

indicate that CaMKII phosphorylation specifically mediates tag setting.

STO-609 blocks late-LTP but permits a pathway tetanized in its presence to display late-LTP provided an independent pathway is tetanized strongly

The CaMKK–CaMKIV pathway mediates CREB phosphorylation and neuronal activity gene transcription (Bito et al., 1996; Ho et al., 2000; Kang et al., 2001). However, it has not been formally addressed before whether a CaMKK–CaMKIV–pCREB pathway might contribute to the regulation of PRP availability. Three-pathway protocols were then used to examine the contribution to late-LTP the CaMKK–CaMKIV-dependent pathway. We used the CaMKK inhibitor STO-609 (Tokumitsu et al., 2002). We first confirmed that STO-609 (5 μM) blocks the late phase of LTP (S1 compared with baseline in Fig. 5*A*, $p > 0.05$). Because STO-609 has little effect on CaMKII activity (Fig. 3*C*,*D*), our perspective is that STO-609 may block late-LTP through a selective effect on the synthesis or distribution of PRPs. To test this, we therefore made the drug present during the weak tetanization of pathway S2 and then washed it out before strong tetanization was applied to pathway S1. In this weak-before-strong protocol, we observed a rescue of early-LTP into late-LTP on the weakly stimulated pathway S2 (compared with baseline in Fig. 5*B*, $p < 0.05$). This was not attributable to some cryptic "potentiating" effect of STO-609, because giving this drug during weak tetanization of a single pathway was without effect on its decay to baseline (Fig. 5*C*, $p > 0.05$). Thus, STO-609 blocks late-LTP without effect on tag setting. The STC theory holds that it must be attributable to limiting the synthesis or availability of PRPs via inhibition of the CaMKK-dependent pathway. We tested this directly using a standard "strong-before-strong" STC protocol in which STO-609 was present during the first strong tetanization but not during the second one. In support of our interpretation, pathway S1 showed late-LTP (compared with baseline in Fig. 5*D*, $p < 0.01$). Supplemental experiments using a weak-before-strong protocol with STO-609 present during strong tetanization revealed no late-LTP on the weakly stimulated pathway, also in keeping with this interpretation [supplemental Fig. S4 (available at www.jneurosci.org as supplemental material), $p > 0.05$].

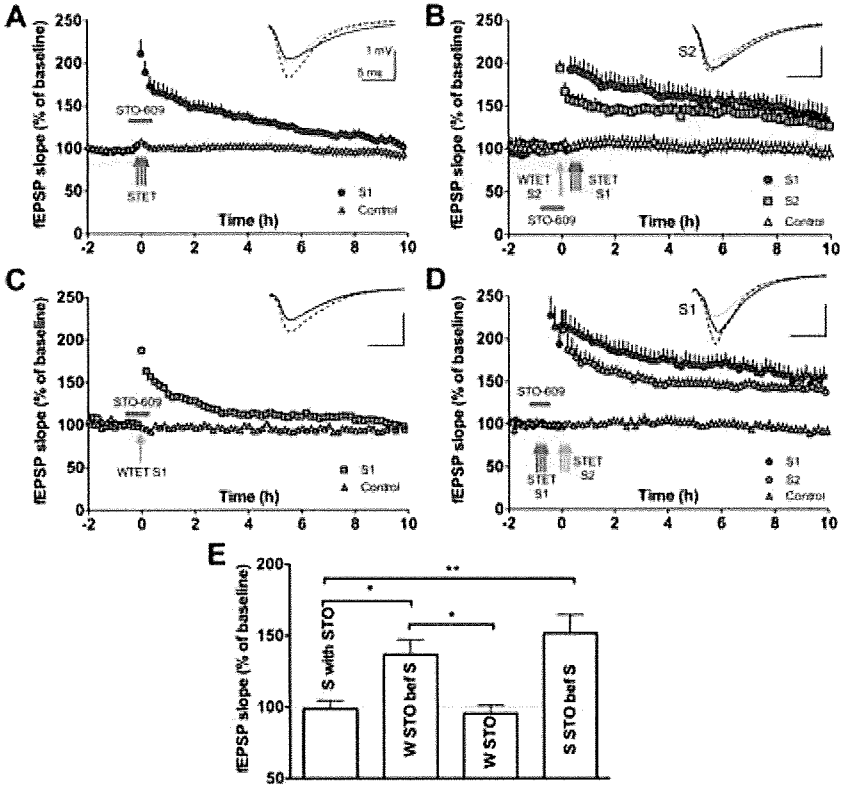

Figure 5. STO-609 dissects a role for CaMKK in a cell-wide process necessary for late-LTP. ***A***, The CaMKK inhibitor STO-609 (5 μM) present at the time of induction blocks late-LTP (S1 vs control pathway at 10 h, $t = 1$, $p \geq 0.05$; $n = 6$). ***B***, Weakly tetanized synapses show late-LTP when STO-609 is applied during the weak tetanus and then removed before strong stimulation is delivered to an independent pathway (S2 vs control pathway, $t = 2.7$, $p \leq 0.05$; stable from 2 to 10 h, $t = 2$, $p \geq 0.05$; $n = 5$). ***C***, STO-609 has no effect on a weakly tetanized pathway S1 (S1 vs baseline at 10 h, $t = 0.65$, $p > 0.05$; $n = 6$). ***D***, In a strong-before-strong protocol, STO-609 given tetanization to S1 does not prevent that pathway showing late-LTP if, after drug washout, strong tetanization is delivered to a second S2 pathway (S1 vs baseline at 10 h, $t = 5$, $p < 0.01$; $n = 6$). ***E***, Bar graph showing differences in the level of potentiation 10 h after stimulation between the four different conditions presented in ***A–D*** (one-way ANOVA, $F = 9.82$, $p < 0.001$). Strong tetanization in the presence of STO-609 fails to produce late-LTP, whereas sets of synapses that received weak tetanization in the presence of STO-609 succeed in maintaining late-LTP if within 20 min a strong tetanus is applied to a second convergent pathway (strong with STO-609 compared with weak tetanus with STO-609 rescued by a strong tetanus, $t = 2.87$, $p < 0.05$). This late-LTP is larger than when no strong tetanus accompanies the weak stimulation (weak tetanus with STO-609 rescued by a strong tetanus compared with weak with STO-609 alone, $t = 3.11$, $p < 0.05$). The effect of STO-609 on a strongly tetanized pathway can be prevented by a strong tetanus to another set of synapses (strong tetanus with STO-609 compared with strong tetanus with STO-609 rescued by a strong tetanus, $t = 4.17$, $p < 0.01$). Error bars indicate SEM. $^*p < 0.05$; $^{**}p < 0.01$. Symbols as in Figure 2. STET, Strong tetanization; WTET, weak tetanization.

KN-93 at 10 μM has less selectivity and blocks both tag setting and PRPs

We conducted three additional control studies. First, our cell-culture data indicate that KN-93 blocks the phosphorylation of CREB at high but not low concentrations (Fig. 3*A*,*B*). Accordingly, we can make the additional prediction that the relative selectivity of a 1 μM concentration of KN-93 on tag setting would be lost if the concentration was increased to 10 μM. Specifically, a higher concentration of KN-93 should block both tag setting and PRP synthesis and availability. Using the same strong-before-weak protocol as the one described in Figure 4, 10 μM KN-93 still blocked late-LTP of the strongly stimulated pathway S1 (compare baseline and control pathway in Fig. 6*A*, $p > 0.05$), but pathway S2 that was weakly tetanized after KN-93 washout now also failed to maintain its potentiation (compare baseline and control pathway in Fig. 6*A*, $p > 0.05$). The interpretation of this result relies on the complete washout of KN-93 by the time the weak tetanus is delivered. As explained in Materials and Methods, our setup allows for >15 washes of the aCSF volume in the experimental chamber between the removal of the drug and the weak tetanization. So as not to rely only on the findings of Figure 4*C*, the same pattern of results was obtained using the weak-before-strong protocol, in which the weak tetanization is delivered before the application of KN-93 (10 μM KN-93 blocked late-LTP in both the strong and weakly tetanized pathways) (Fig. 6*B*, $p > 0.05$). A parsimonious explanation for this would be the contribution of

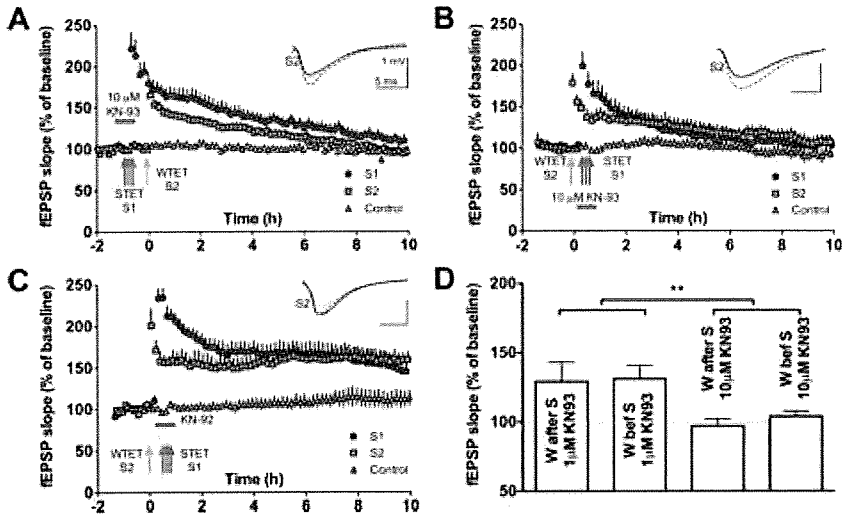

Figure 6. A higher concentration of KN-93 has less selective effects than a lower concentration. ***A***, ***B***, Higher concentrations of KN-93 fail to dissociate synapse-specific and cell-wide processes in late-LTP, in contrast to data in Figure 2 with 1 μM KN-93. ***A***, A weakly stimulated pathway (S2) failed to show late-LTP (S2 vs control 10 h, $t = 0.1, p \geq 0.05$) when the stimulation was given 20 min after a strong tetanus to S1 if the higher concentration of 10 μM KN-93 was present during LTP induction. The strongly stimulated pathway also fails to show late-LTP (S1 vs control 10 h, $t = 1.4, p \geq 0.05; n = 9$). ***B***, The rescue of early-LTP into late-LTP is also not seen in S2 (S2 vs control 10 h, $t = 1.7, p \geq 0.05$) if tetanization is given when 10 μM KN-93 is present during S1. S1 also fails to maintain late-LTP (S1 vs control 10 h, $t = 0.9, p \geq 0.05; n = 7$). ***C***, The rescue of early-LTP into late-LTP in a weakly tetanized pathway (S2) is seen even if S1 strong tetanization is delivered when KN-92 is present (S2 vs control 10 h after tetanus, $t = 3.5, p < 0.01; n = 5$). ***D***, Bar graph showing differences in the level of potentiation 10 h after stimulation between the two concentrations of KN-93 used in Figures 4 and 6 (two-way ANOVA, $F = 7.7, p < 0.01$). The order of stimulation and drug application had no effect ($F = 0.14$, $p > 0.05$). Error bars indicate SEM. $^{**}p < 0.01$. Symbols as in Figure 2. STET, Strong tetanization; WTET, weak tetanization.

KN-93-sensitive CaM kinase(s) distinct from CaMKII, such as the CaMKK–CaMKIV pathway, with respect to PRP availability.

The second control study is for nonspecific effects of KN-93. We did this using the inactive analog KN-92 (10 μM). Using a weak-before-strong protocol, KN-92 did not prevent the rescue of early-LTP on a weakly tetanized pathway S2 when given in the presence of strong tetanization on S1 (Fig. 6*C*, $p < 0.01$).

Third, we checked that KN-93 would still block tag setting at a high concentration. In previous work (Sajikumar and Frey, 2007), a strong-before-strong protocol was used to examine the effect of KN-62 (1-[*N*,*O*-bis(5-isoquinolinesulphonyl)-*N*-methyl-L-tyrosyl]-4-phenylpiperazine) (an alternative inhibitor of CaM kinases) on late-LTP, finding evidence for a role in tag setting. The strong-before-strong protocol is sufficient to identify a role in tag setting, although not as analytically powerful as the strong-before-weak protocols. Nonetheless, we observed that, if present at the time of induction, a 10 μM concentration of KN-93 blocked late-LTP at 10 h [pathway S2 compared with baseline in supplemental Fig. S5*A* (available at www.jneurosci.org as supplemental material), $p > 0.05$] but had no effect on the induction of LTP on a pathway tetanized 20 min earlier [pathway S1 compared with baseline in Fig. S5*A* (available at www.jneurosci.org as supplemental material), $p < 0.01$]. In separate experiments, the order was reversed and the same dose of KN-93 was present during the first tetanization but was then washed out. Late-LTP on the pathway tetanized under 10 μM KN-93 failed to show any potentiation 10 h after tetanus when compared with a control baseline [pathway S1 in supplemental Fig. S5*B* (available at www.jneurosci.org as supplemental material), $p > 0.05$]. However, after 20 min of aCSF flow into the chamber that successfully washed out KN-93, tetanization of the second pathway induced robust late-LTP lasting 10 h [pathway S2 in supplemental Fig. S5*B* (available at www.jneurosci.org as supplemental material), $p < 0.01$]. Also, KN-92 did not impair late-LTP if present during strong tetanization [compare baseline and control pathway in supplemental Fig. S5*C* (available at www.jneurosci.org as supplemental material), $p < 0.01$].

Discussion

These experiments have identified dissociable roles specific for distinct CaM kinase pathways in the persistence of synaptic potentiation, and they provide new molecular insights on the requirement for synapse-specific and cell-wide mechanisms mediating late-LTP. Our findings emerge from our use of long time course three-pathway protocols (i.e., two pathways tetanized in weak-before-strong and strong-before-weak modes, with a third nontetanized control pathway), which were readily combined with fast wash-in/washout pharmacological treatments. First, we confirm previous observations (Frey and Morris, 1997; Fonseca et al., 2004) that early-LTP induced at one set of synapses can be rescued into late-LTP if, within a short time window (Frey and Morris, 1998a), late-LTP is induced at another set of synapses in the same CA1 neuronal population (Fig. 2). Second, cell-biological data reveals differential concentration-dependent effects of KN-93 and STO-609 on two complementary requirements for the maintenance of LTP, with 1 μM KN-93 having specific effects on phosphorylation of CAMKII, whereas higher concentrations also affected pCREB, with STO-609 having no affect on pCaMKII (Fig. 3). Third, the low concentration of KN-93 selectively interrupted a pathway-specific tagging process but spared the availability of PRPs, as analytically revealed by successful late-LTP after weak tetanization of a second independent pathway (Fig. 4). A separate CaMKII inhibitor, Myr-AIP, had similar actions (supplemental Fig. S3, available at www.jneurosci.org as supplemental material). Fourth, STO-609 was shown to block late-LTP but to spare the setting of synaptic tags (Fig. 5). Fifth, consistent with dose–response profile shown in the cell-culture immunocytochemistry, we observed that a higher concentration of KN-93 blocked late-LTP but did so by both blocking tagging and other cell-wide mechanisms (Fig. 6), a result that builds on previous work with KN-62 (Sajikumar et al., 2007).

The synaptic tagging and capture hypothesis provides the key concepts that are central to our analysis of the rescue of early-LTP into late-LTP (Frey and Morris, 1998b). Indeed, this hypothesis asserts and predicts two requirements for long-term changes in synaptic efficacy: (1) the local setting of tags at stimulated synapses, and (2) the cell-wide or dendritic-domain-wide availability of PRPs that can be captured by the tags and so enable mechanisms responsible for the stabilization of potentiation (Reymann and Frey, 2007). However, the signal transduction pathways mediating these two requirements have remained unclear. Amid the potentially numerous molecular players and complex interactions involved in these processes, some may be

required for both tag setting and PRP availability [e.g., activation of NMDA receptors (O'Carroll and Morris, 2004)]. Other molecules (or molecular states, such as phosphorylation) may only be necessary for tag setting and yet others only for PRP synthesis and/or their availability (supplemental Fig. S1, available at www.jneurosci.org as supplemental material). Our experiments identify a dissociable molecular cascade within the CaM kinase pathways for both tag setting and PRP supply.

Specific targeting of tag setting using a low concentration of KN-93 and of PRP synthesis using STO-609

CaMKII is a broad-range kinase that regulates many neuronal functions (Erondu and Kennedy, 1985; Braun and Schulman, 1995; Yamauchi, 2005). In the CA3 to CA1 Schaffer-collateral pathway of the hippocampus, CaMKII activation by Ca^{2+}/CaM is required at the time of LTP induction (Malenka et al., 1989) and, as shown recently, remains necessary during the maintenance of LTP (Sanhueza et al., 2007). Compelling evidence indicates that a dodecameric holoenzyme is activated by intersubunit phosphorylation in the presence of calcium/calmodulin (Miller and Kennedy, 1986; Hanson et al., 1994). According to this model, during a robust Ca^{2+} signal, the binding of calmodulin to each subunit unmasks the kinase domain by repelling the autoinhibitory domain of CaMKII but also exposing a threonine 286 site (Thr-286) in the adjacent subunit. The subsequent phosphorylation of Thr-286 then generates an autonomous kinase activity and also increases the affinity for calmodulin and creating a state in which calmodulin is transiently trapped by CaMKII even shortly after the end of a Ca^{2+} transient (Meyer et al., 1992). It has been proposed that this property may enable active CaMKII to translocate into the spine (Zhang et al., 2008) and for autophosphorylated CaMKII to act as a switch capable of maintaining changes in synapse efficacy (Lisman and Goldring, 1988; Lisman and Zhabotinsky, 2001; Miller et al., 2005). This switch could, in principle, also participate in tag setting and/or the local capture of available PRPs (Sajikumar et al., 2007).

To secure definitive evidence for these ideas, we developed a long time course three-pathway slice recording protocol and then conducted robust differential CaMK pharmacological experiments whose aim was to experimentally dissociate tag setting and PRP supply. Our key observations are that (1) a low dose of KN-93, which interferes with the phosphorylation of CaMKII in cell culture but spares most CREB phosphorylation, has the effect of specifically inhibiting tag setting while allowing PRP availability heterosynaptically, whereas (2) STO-609 selectively affects CREB phosphorylation but not pCaMKII and blocks PRP availability without affecting tag setting.

The value of 10 h experiments and fast-reversible pharmacological interventions

The present findings underwrite the value of allowing newly prepared brain slices, subject to minimal test stimulation, to stabilize for at least 4 h before tetanization, as long recommended by the Frey group in Magdeburg, Germany. Biochemical data suggest that it can take hours before kinase activation levels stabilize after slice preparation (Ho et al., 2004) and that low frequencies of test stimulation cause minimal interference with PRP availability (Fonseca et al., 2006). We also recorded for much longer periods than is typical in many LTP experiments, making it desirable, if not essential, to have a third nontetanized control pathway. Our data provide additional indications that the dynamic interactions set in train by tetanization continue for several hours (e.g., in Fig. 4*B*, the crossover of the strong and weakly tetanized pathways takes place over a period from 2 to 6 h after tetanization, and the strongly tetanized pathway does not decay to baseline until 8–10 h have elapsed). These points may seem merely methodological but, in our view, have been critical to dissecting the differential role of distinct CaM kinases with respect to synaptic tagging and capture.

It is unfortunate that we could not use brain slices from mice subject to gene targeting of the calcium/calmodulin pathway (Giese et al., 1998). The reason is that the dissociation of tag setting and PRP synthesis requires the differential inhibition of different components of CaMK pathways to be rapidly reversible. A pharmacological approach was essential, although we anticipate that our approach could be complemented by observations on suitable genetic reporter mice in the future.

Multiple dissociable CaMK pathways contribute to STC

Despite a large body of work on activity-dependent transcription/translation during long-term plasticity, surprisingly little has been elucidated on their relationship to the concrete implementation of long-lasting synaptic modifications. The evidence presented here suggests that STC may operate at least in part via two related yet distinct limbs of CaMK signaling: tag setting by CaMKII and activity-dependent gene transcription regulation by a CaMKK-dependent pathway. This new model nicely accounts for the interactive yet orthogonal (synapse-specific vs cell-wide) nature of tag setting and PRP synthesis, which might be coregulated in parallel via distinct pools of Ca^{2+}/CaM. However, the molecular basis of the tag–PRP interactions remains unclear. Better understanding of CaMKII dynamics (kinase activity and kinase content) and molecular dissection of the CaMKII-containing protein complexes at activated synapses will clearly be important steps toward solving this issue (Lisman et al., 2002; Yamauchi, 2005).

Because our data here establish the necessity for CaMKII activation to initiate the tag-setting process, one attractive idea is to consider that perhaps autophosphorylation of CaMKII itself might constitute the "tag" or be an integral part of it. However, independent studies have also shown evidence suggesting that pCaMKII signal may sometimes spread beyond the area of the originally stimulated synapses (Ouyang et al., 1997; Rose et al., 2009). The mechanistic basis for such potential loss of input specificity at the pCaMKII level remains unsolved. Additional studies are needed to resolve this apparent contradiction and pin down the molecular identity of the tag set in motion by CaMKII activation.

The wider implications of this work for the neurobiology of memory are of considerable interest. It provides a candidate mechanism for how inconsequential events (mimicked by weak stimulation in the protocols used here) may be remembered for much longer when they occur against the background of other surprising or emotionally significant events (mimicked by strong stimulation here), as occurs in flashbulb memory situations. Definitive evidence will require demonstration of STC *in vivo* and the creation of behavioral paradigms to investigate the transformation of short-term into long-term memory in complementary situations (Moncada and Viola, 2007).

References

Andersen P, Sundberg SH, Sveen O, Wigström H (1977) Specific long-lasting potentiation of synaptic transmission in hippocampal slices. Nature 266:736–737.

Bito H, Deisseroth K, Tsien RW (1996) CREB phosphorylation and dephosphorylation: a Ca^{2+}- and stimulus duration-dependent switch for hippocampal gene expression. Cell 87:1203–1214.

Bliss TV, Lomo T (1973) Long-lasting potentiation of synaptic transmission in the dentate area of the anaesthetized rabbit following stimulation of the perforant path. J Physiol 232:331–356.

Braun AP, Schulman H (1995) The multifunctional calcium/calmodulin-dependent protein kinase: from form to function. Annu Rev Physiol 57:417–445.

Erondu NE, Kennedy MB (1985) Regional distribution of type II Ca^{2+}/calmodulin-dependent protein kinase in rat brain. J Neurosci 5:3270–3277.

Fonseca R, Nägerl UV, Morris RG, Bonhoeffer T (2004) Competing for memory: hippocampal LTP under regimes of reduced protein synthesis. Neuron 44:1011–1020.

Fonseca R, Nägerl UV, Bonhoeffer T (2006) Neuronal activity determines the protein synthesis dependence of long-term potentiation. Nat Neurosci 9:478–480.

Frey U, Morris RGM (1997) Synaptic tagging and long-term potentiation. Nature 385:533–536.

Frey U, Morris RGM (1998a) Weak before strong: dissociating synaptic tagging and plasticity-factor accounts of late-LTP. Neuropharmacology 37:545–552.

Frey U, Morris RGM (1998b) Synaptic tagging: implications for late maintenance of hippocampal long-term potentiation. Trends Neurosci 21:181–188.

Frey U, Krug M, Reymann KG, Matthies H (1988) Anisomycin, an inhibitor of protein synthesis, blocks late phases of LTP phenomena in the hippocampal CA1 region in vitro. Brain Res 452:57–65.

Giese KP, Fedorov NB, Filipkowski RK, Silva AJ (1998) Autophosphorylation at Thr286 of the alpha calcium-calmodulin kinase II in LTP and learning. Science 279:870–873.

Hansel C, de Jeu M, Belmeguenai A, Houtman SH, Buitendijk GH, Andreev D, De Zeeuw CI, Elgersma Y (2006) alphaCaMKII Is essential for cerebellar LTD and motor learning. Neuron 51:835–843.

Hanson PI, Meyer T, Stryer L, Schulman H (1994) Dual role of calmodulin in autophosphorylation of multifunctional CaM kinase may underlie decoding of calcium signals. Neuron 12:943–956.

Ho N, Liauw JA, Blaeser F, Wei F, Hanissian S, Muglia LM, Wozniak DF, Nardi A, Arvin KL, Holtzman DM, Linden DJ, Zhuo M, Muglia LJ, Chatila TA (2000) Impaired synaptic plasticity and cAMP response element-binding protein activation in Ca^{2+}/calmodulin-dependent protein kinase type IV/Gr-deficient mice. J Neurosci 20:6459–6472.

Ho OH, Delgado JY, O'Dell TJ (2004) Phosphorylation of proteins involved in activity-dependent forms of synaptic plasticity is altered in hippocampal slices maintained in vitro. J Neurochem 91:1344–1357.

Ishida A, Kameshita I, Okuno S, Kitani T, Fujisawa H (1995) A novel highly specific and potent inhibitor of calmodulin-dependent protein kinase II. Biochem Biophys Res Commun 212:806–812.

Kang H, Sun LD, Atkins CM, Soderling TR, Wilson MA, Tonegawa S (2001) An important role of neural activity-dependent CaMKIV signaling in the consolidation of long-term memory. Cell 106:771–783.

Kawashima T, Okuno H, Nonaka M, Adachi-Morishima A, Kyo N, Okamura M, Takemoto-Kimura S, Worley PF, Bito H (2009) Synaptic activity-responsive element in the Arc/Arg3.1 promoter essential for synapse-to-nucleus signaling in activated neurons. Proc Natl Acad Sci U S A 106:316–321.

Krug M, Lössner B, Ott T (1984) Anisomycin blocks the late phase of long-term potentiation in the dentate gyrus of freely moving rats. Brain Res Bull 13:39–42.

Leutgeb JK, Frey JU, Behnisch T (2003) LTP in cultured hippocampal-entorhinal cortex slices from young adult (P25-30) rats. J Neurosci Methods 130:19–32.

Lisman J, Schulman H, Cline H (2002) The molecular basis of CaMKII function in synaptic and behavioural memory. Nat Rev Neurosci 3:175–190.

Lisman JE, Goldring MA (1988) Feasibility of long-term storage of graded information by the Ca^{2+}/calmodulin-dependent protein kinase molecules of the postsynaptic density. Proc Natl Acad Sci U S A 85:5320–5324.

Lisman JE, Zhabotinsky AM (2001) A model of synaptic memory: a CaMKII/PP1 switch that potentiates transmission by organizing an AMPA receptor anchoring assembly. Neuron 31:191–201.

Malenka RC, Kauer JA, Perkel DJ, Mauk MD, Kelly PT, Nicoll RA, Waxham MN (1989) An essential role for postsynaptic calmodulin and protein kinase activity in long-term potentiation. Nature 340:554–557.

Malinow R, Schulman H, Tsien RW (1989) Inhibition of postsynaptic PKC or CaMKII blocks induction but not expression of LTP. Science 245:862–866.

Martin KC, Casadio A, Zhu H, Yaping E, Rose JC, Chen M, Bailey CH, Kandel ER (1997) Synapse-specific, long-term facilitation of aplysia sensory to motor synapses: a function for local protein synthesis in memory storage. Cell 91:927–938.

Meyer T, Hanson PI, Stryer L, Schulman H (1992) Calmodulin trapping by calcium-calmodulin-dependent protein kinase. Science 256:1199–1202.

Miller P, Zhabotinsky AM, Lisman JE, Wang XJ (2005) The stability of a stochastic CaMKII switch: dependence on the number of enzyme molecules and protein turnover. PLoS Biol 3:e107.

Miller SG, Kennedy MB (1986) Regulation of brain type II Ca^{2+}/calmodulin-dependent protein kinase by autophosphorylation: a Ca^{2+}-triggered molecular switch. Cell 44:861–870.

Moncada D, Viola H (2007) Induction of long-term memory by exposure to novelty requires protein synthesis: evidence for a behavioral tagging. J Neurosci 27:7476–7481.

Navakkode S, Sajikumar S, Frey JU (2007) Synergistic requirements for the induction of dopaminergic D1/D5-receptor-mediated LTP in hippocampal slices of rat CA1 in vitro. Neuropharmacology 52:1547–1554.

O'Carroll CM, Morris RGM (2004) Heterosynaptic co-activation of glutamatergic and dopaminergic afferents is required to induce persistent long-term potentiation. Neuropharmacology 47:324–332.

Ouyang Y, Kantor D, Harris KM, Schuman EM, Kennedy MB (1997) Visualization of the distribution of autophosphorylated calcium/calmodulin-dependent protein kinase II after tetanic stimulation in the CA1 area of the hippocampus. J Neurosci 17:5416–5427.

Reymann KG, Frey JU (2007) The late maintenance of hippocampal LTP: requirements, phases, "synaptic tagging", "late-associativity" and implications. Neuropharmacology 52:24–40.

Rose J, Jin SX, Craig AM (2009) Heterosynaptic molecular dynamics: locally induced propagating synaptic accumulation of CaM kinase II. Neuron 61:351–358.

Sajikumar S, Navakkode S, Frey JU (2005) Protein synthesis-dependent long-term functional plasticity: methods and techniques. Curr Opin Neurobiol 15:607–613.

Sajikumar S, Navakkode S, Frey JU (2007) Identification of compartment- and process-specific molecules required for "synaptic tagging" during long-term potentiation and long-term depression in hippocampal CA1. J Neurosci 27:5068–5080.

Sajikumar S, Navakkode S, Frey JU (2008) Distinct single but not necessarily repeated tetanization is required to induce hippocampal late-LTP in the rat CA1. Learn Mem 15:46–49.

Sanhueza M, McIntyre CC, Lisman JE (2007) Reversal of synaptic memory by Ca^{2+}/calmodulin-dependent protein kinase II inhibitor. J Neurosci 27:5190–5199.

Schurr A, Reid KH, Tseng MT, Edmonds HL Jr, West CA, Rigor BM (1986) Effect of electrical stimulation on the viability of the hippocampal slice preparation. Brain Res Bull 16:299–301.

Schwartzkroin PA, Wester K (1975) Long-lasting facilitation of a synaptic potential following tetanization in the in vitro hippocampal slice. Brain Res 89:107–119.

Sumi M, Kiuchi K, Ishikawa T, Ishii A, Hagiwara M, Nagatsu T, Hidaka H (1991) The newly synthesized selective Ca^{2+}/calmodulin dependent protein kinase II inhibitor KN-93 reduces dopamine contents in PC12h cells. Biochem Biophys Res Commun 181:968–975.

Tokumitsu H, Inuzuka H, Ishikawa Y, Ikeda M, Saji I, Kobayashi R (2002) STO-609, a specific inhibitor of the Ca^{2+}/calmodulin-dependent protein kinase kinase. J Biol Chem 277:15813–15818.

Yamauchi T (2005) Neuronal Ca^{2+}/calmodulin-dependent protein kinase II—discovery, progress in a quarter of a century, and perspective: implication for learning and memory. Biol Pharm Bull 28:1342–1354.

Zhang YP, Holbro N, Oertner TG (2008) Optical induction of plasticity at single synapses reveals input-specific accumulation of αCaMKII. Proc Natl Acad Sci U S A 105:12039–12044.